Encapsulation of tricopper cluster in a protein-like cavitand enables facile redox processes from Cu^{I}Cu^{I}Cu^I to Cu^{II}Cu^{II}Cu^{II} states

Weiyao Zhang,[†] Curtis E. Moore,[†] and Shiyu Zhang*,[†]

[†]Department of Chemistry & Biochemistry, The Ohio State University, 100 West 18th Avenue, Columbus, Ohio 43210, United States

ABSTRACT: One-pot reaction of tris(2-aminoethyl)amine (TREN), [Cu^I(MeCN)$_4$]PF$_6$, and paraformaldehyde affords a mixed-valent [**TREN$_4$**Cu^{II}Cu^{I}Cu^I(μ_3-OH)](PF$_6$)$_3$ complex. The macrocyclic azacryptand **TREN$_4$** contains four TREN motifs, three of which provide a bowl-shape binding pocket for the [Cu$_3$(μ_3-OH)]$^{3+}$ core. The fourth TREN caps on top of the tricopper cluster to form a cavitand, imposing conformational constraints and preventing solvent interaction. Contrasting the limited redox capability of synthetic tricopper complexes reported so far, [**TREN$_4$**Cu^{II}Cu^{I}Cu^I(μ_3-OH)](PF$_6$)$_3$ exhibits several reversible single-electron redox events. The distinct electrochemical behaviors of [**TREN$_4$**Cu^{II}Cu^{I}Cu^I(μ_3-OH)](PF$_6$)$_3$ and its solvent-exposed analog [**TREN$_3$**Cu^{II}Cu^{II}Cu^{II}(μ_3-O)](PF$_6$)$_4$ suggest that isolation of tricopper core in a protein-like cavitand enables facile electron transfer, allowing potential application of synthetic tricopper complexes as redox catalysts. Indeed, the fully reduced [**TREN$_4$**Cu^{I}Cu^{I}Cu^I(μ_3-OH)](PF$_6$)$_2$ can reduce O$_2$ under acidic conditions. The geometric constraints provided by the cavitand are reminiscent of Nature's multicopper oxidases (MCOs). For the first time, a synthetic tricopper cluster was isolated and fully characterized at Cu^{I}Cu^{I}Cu^I (**4a**), Cu^{II}Cu^{I}Cu^I (**4b**), and Cu^{II}Cu^{II}Cu^I state (**4c**), providing structural and spectroscopic models for many intermediates in MCOs. Fast electron transfer rates (10^5 - 10^6 M^{-1}s^{-1}) were observed for both Cu^{I}Cu^{I}Cu^I/Cu^{II}Cu^{I}Cu^I and Cu^{II}Cu^{I}Cu^I/Cu^{II}Cu^{II}Cu^I redox couples, approaching the rapid electron transfer rates of copper sites in MCO.

INTRODUCTION

Synthetic tricopper clusters have been a prominent synthetic target for (bio)inorganic community over the past few decades,[1–9] since tricopper centers were identified/proposed as essential active sites for biological reduction of O$_2$ to H$_2$O in multicopper oxidase (MCO)[10,11] and aerobic hydroxylation of methane in particulate methane monooxygenase (pMMO).[12] Although a tricopper active site in pMMO has been disputed, the conversion of methane to methanol was demonstrated with small-molecule tricopper complexes.[13,14] In both oxygen reduction and hydrocarbon hydroxylation, the synergy of three Cu^{II}/Cu^I redox couples in tricopper clusters is essential to harness the oxidative power of O$_2$. Therefore, understanding factors governing the redox of tricopper clusters as a single unit is fundamental to their development as biomimetic catalysts in fuel cell technology and functionalization of alkanes.

An ideal tricopper redox catalyst should be able to engage all three Cu^{II}/Cu^I couple and accommodate four redox states from Cu^{I}Cu^{I}Cu^I to Cu^{II}Cu^{II}Cu^{II}. However, the majority of synthetic tricopper clusters reported to date have limited redox capability, and only isolated at a single oxidation state (primarily Cu^{II}Cu^{II}Cu^{II} or Cu^{I}Cu^{I}Cu^I).[15,16] Copper(I) center (d^{10}) and copper(II) center (d^9) prefer distinct geometry due to the Jahn-Teller effect. The redox of Cu^{II}/Cu^I, in an unconstrained solvent-exposed environment, often results in significant geometric rearrangement associated with high reorganization energy.[17] Notably, among *ca.* 186 crystallographically characterized molecular tricopper μ_3-E, (E= O, OH, S) clusters, **1** and **2**
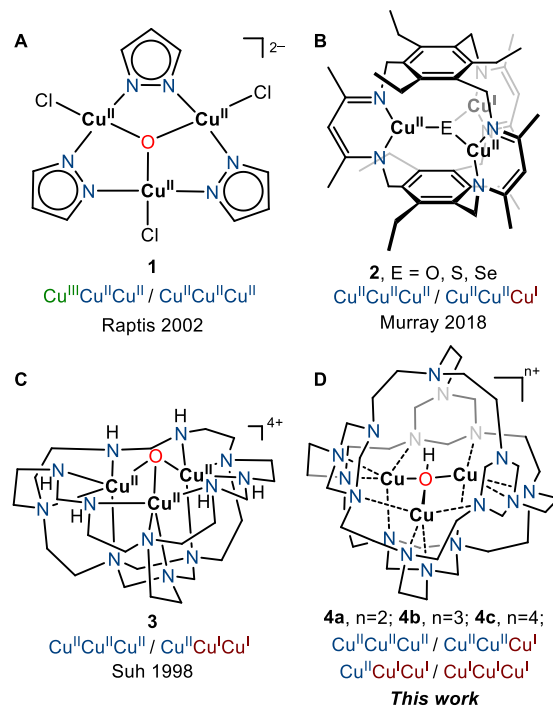

Figure 1. Redox-active tricopper clusters and their corresponding oxidation states demonstrated by cyclic voltammetry. Complex **4** reported in this work was isolated and characterized at three different oxidation states, denoted as **4a** (Cu^{I}Cu^{I}Cu^I), **4b** (Cu^{II}Cu^{I}Cu^I), and **4c** (Cu^{II}Cu^{II}Cu^I).

(Figure 1A, 1B) represents the only two redox-active examples.[18,19] Even **1** and **2**, however, cannot be further reduced to the $Cu^ICu^ICu^I$ state,[16] which is crucial for the activation of O_2 during catalytic oxygen reduction reaction (ORR) and hydrocarbon hydroxylation. In sharp contrast, Nature's trinuclear copper cluster (TNC) in MCOs has been observed in three different oxidation states: fully reduced ($Cu^ICu^ICu^I$, FR), alternative resting ($Cu^{II}Cu^ICu^I$, AR), and native intermediate ($Cu^{II}Cu^{II}Cu^{II}$, NI). Unlike synthetic tricopper complexes, TNC is embedded in a protein matrix, which provides conformational strains and site isolation that reduce reorganization energy during electron transfer (ET).[20,21]

According to Marcus theory, electron transfer in solution is strongly influenced by both inner sphere ligand interactions and outer sphere solvent environments.[17] We posited that the encapsulation of synthetic tricopper center in a protein-like cavitand could constrain the coordination environment, hence lowing the barriers for reorganization and allowing access to different redox states of tricopper clusters. Instead of using bulky ligands to simulate the protein environment, we leveraged multicyclic azacryptand ligand to restrict the conformational freedom and limit solvent interaction. The electrochemical property of **4** was compared to their solvent-exposed analog [**TREN$_3$**$Cu^{II}Cu^{II}Cu^{II}$(μ_3-O)](PF$_6$)$_4$, **3**[22] to understand how compartmentalization of tricopper center impacts the redox behavior of Cu^{II}/Cu^I.

RESULTS AND DISCUSSION

Synthesis and characterization of encapsulated tricopper complex, [TREN$_4$Cu^{II}Cu^{I}Cu^I(μ_3-OH)](PF$_6$)$_3$, 4b. Tricopper complex [**TREN$_3$**$Cu^{II}Cu^{II}Cu^{II}$(μ_3-O)](PF$_6$)$_4$, **3** (Figure 1C) has been considered as a structural[22] and spectroscopic model[23,24] for TNC. However, **3** do not exhibit the multi-electron redox function of TNC. The *ca.* 550 mV separation of the redox couple (see supporting information), which is typical for synthetic tricopper complexes, indicates a substantial barrier for

reorganization during ET. Notably, the reduction of $Cu^{II}Cu^ICu^I$ to $Cu^ICu^ICu^I$ was not observed within the voltage window of water, suggesting **3** is not suitable to activate dioxygen. To construct a protein-like environment, we sought to install an additional TREN cap on **3** to afford **4** (Figure 1D). The desired azacryptand ligand **TREN$_4$** has synthesized previously,[25] however, no transition metal complex has been reported thus far. We found that metalation of **TREN$_4$** with Cu(I) and Cu(II) salts only afforded complicated mixtures in low yields. Inspired by the metal-templated synthesis reported by Suh et. al.,[22] we explored the one-pot reaction of copper salts, TREN, and paraformaldehyde. Reaction of [Cu^I(MeCN)$_4$]PF$_6$, TREN (3.3 equivalents), and paraformaldehyde (20 equivalents based on CH_2O units) resulted in the formation of a blue solid (Figure 2A). Workup and recrystallization under our optimized conditions afforded complex **4b** in 18% yield (see supporting information).

The Electrospray Ionization Mass Spectrum (ESI-MS, Figure 2B) of **4b** exhibited a prominent peak at 312.2 m/z, and the isotope distribution pattern matches that of [**TREN$_4$**$Cu^{II}Cu^ICu^I$(μ_3-OH)]$^{3+}$ (molecular mass = 938.75 g/mol, C$_{36}$H$_{75}$Cu$_3$N$_{16}$O), supporting the presence of a [Cu$_3$(μ_3-OH)]$^{3+}$ core. The frozen solution electron paramagnetic resonance (EPR) spectrum of **4b** (Figure 2C) displayed a rhombic signal (g_x = 2.25, g_y = 2.14, g_z = 2.01) with hyperfine couplings to one $^{63/65}$Cu (I = 3/2) nucleus ($A_z(Cu)$ = 146 MHz), suggesting a valence-localized one-hole $Cu^{II}Cu^ICu^I$ electronic structure. The high g_x and g_y values indicated that the unpaired electron resides in the d_{z^2} orbital, consistent with a trigonal bipyramidal geometry.[26]
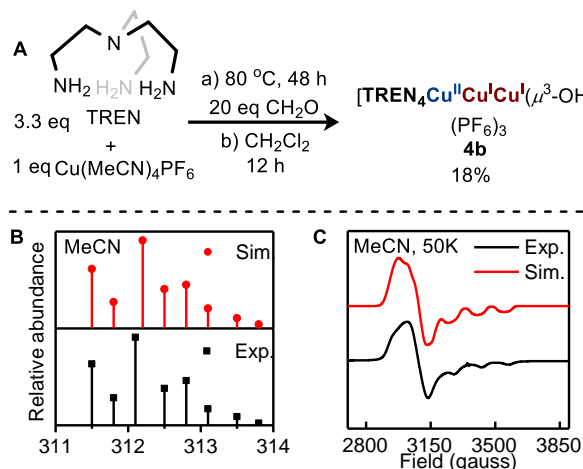

Figure 3. Solid-state structure of **4b** (100 K) with thermal ellipsoids shown at 35% probability level. All PF$_6$ anions, the minor components of disorder, and all C-H hydrogen atoms are omitted for clarity.

Single crystal X-ray diffraction analysis of **4b** confirmed its assignment as mixed-valent [**TREN$_4$**$Cu^{II}Cu^ICu^I$(μ_3-OH)](PF$_6$)$_3$ (Figure 3). Cryptate **4b** shares the macrocyclic tricopper assembly of **3** but features a fully encapsulated tricopper core. Three of four TREN moieties in **TREN$_4$** serve as bowl-shape binding sites for the tricopper core, while the remaining one

Figure 2. (A) Synthesis of [**TREN$_4$**$Cu^{II}Cu^ICu^I$(μ_3-OH)](PF$_6$)$_3$ (**4b**). (B) ESI-MS (positive mode) of **4b**, (C) X-band EPR spectrum (frozen MeCN, 0.5 mM) of **4b**, g_x = 2.25 g_y = 2.14, g_z = 2.01, $A_z(Cu)$ = 146 MHz.
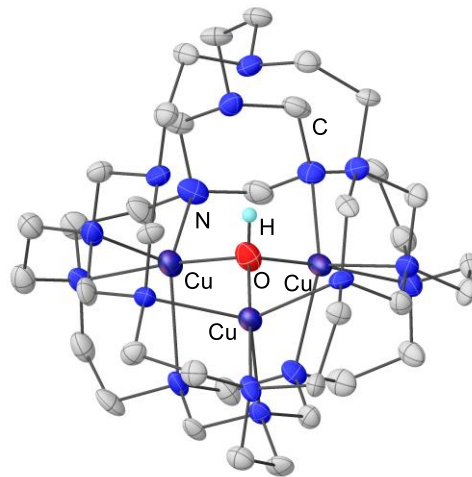
forms a cavitand that isolates the $Cu_3(\mu_3\text{-OH})$ core in a protein-like capsule. With its one-hole $Cu^{II}Cu^ICu^I$ oxidation state, complex **4b** is the first synthetic model for the alternative resting (AR) state in MCO ($Cu^{II}Cu^ICu^I$).[27,28] The Cu⋯Cu and Cu-O bond metrics within **4b** (Cu⋯Cu: 2.973-3.260 Å; Cu-O: 1.878-1.971 Å) are similar to those in **3** (Cu⋯Cu: 3.095 Å; Cu-O: 1.863 Å) but vary greater from each other, perhaps as a result of its localized electronic structure.

Electrochemical study of 4b and 3. To evaluate the impact of tricopper encapsulation on the redox capability, we performed cyclic voltammetry (CV) studies of **3** and **4** in aqueous environments with pH values range from 5.6 to 13. Dissolution of **3** in water produces an equilibrium mixture of **3** and its conjugate acid (pKa = 4.6).[22] Cyclic voltammogram of **3** at pH = 5.6 showed an irreversible reduction at −0.18 V (vs. NHE), which gradually shifts to −0.30 V (vs. NHE) at pH = 13. This cathodic peak is assigned to the two-electron reduction of $[Cu^{II}Cu^{II}Cu^{II}(\mu_3\text{-OH})]^{5+}$ to $[Cu^{II}Cu^ICu^I(\mu_3\text{-OH})]^{3+}$ based on variable scan rate CV study (see supporting information, Figure S19). During the reverse scan, an anodic peak was observed at 0.37 V (vs. NHE, pH = 5.8), which is attributed to the oxidation of $[Cu^{II}Cu^ICu^I(\mu_3\text{-OH})]^{3+}$ back to $[Cu^{II}Cu^{II}Cu^{II}(\mu^3\text{-OH})]^{5+}$ (Figure 4, left). The ca. 550 mV separation of the redox couple indicates a substantial geometric difference at $Cu^{II}Cu^{II}Cu^{II}$ and $Cu^{II}Cu^ICu^I$ states. As the tricopper center in **3** is exposed to bulk exterior, it can lose/gain interactions with solvents during redox processes, further raising the reorganization energy. Notably, further reduction of $[Cu^{II}Cu^ICu^I(\mu_3\text{-OH})]^{3+}$ to $[Cu^ICu^ICu^I(\mu_3\text{-OH})]^{2+}$ was not observed within the voltage window of water. The CV of **3** becomes more reversi-

ble as the pH increases from 5.6 to 13, perhaps due to the deprotonation of central μ_3-OH to μ_3-O, a stronger ligand that rigidifies the coordination environment (see supporting information).

In contrast to the irreversible redox behavior of **3**, the cyclic voltammogram of **4** shows two reversible ($E_{1/2} = -0.55$ V and -0.13 V vs. NHE) and one irreversible ($E_{ox} = 0.33$ V vs. NHE) redox events, allowing access to all four oxidation states of the tricopper cluster electrochemically (Figure 4B). The contrasting electrochemical behaviors of **3** and **4** suggest that the geometric constraints imposed by **TREN₄** reduce the reorganization energies during ET. Additionally, the three redox events of complex **4** are insensitive to the pH of the buffer (Figure 4B), implicating that the protein-like cavitand of **TREN₄** isolates the tricopper core from direct solvent interactions. The CVs of **4b** in aqueous and non-aqueous environments, e.g. dimethylformamide or acetonitrile, are essentially the same (Figure 4C), further supporting that the redox of tricopper center in **4** is unaffected by the bulk exterior.

Synthesis and characterization of 4a ($Cu^ICu^ICu^I$) and 4c ($Cu^{II}Cu^{II}Cu^I$). The highly reversible oxidation and reduction couples of **4b** prompted us to pursue the isolation of fully reduced $[\textbf{TREN}_4Cu^ICu^ICu^I(\mu_3\text{-OH})]^{2+}$ (**4a**) and two-hole $[\textbf{TREN}_4Cu^{II}Cu^{II}Cu^I(\mu_3\text{-OH})]^{4+}$ (**4c**, Figure 4A). Consistent with its electrochemical behavior, chemical oxidation of **4b** with decamethylferrocenium hexafluorophosphate ($Me_{10}FcPF_6$, $E_{1/2} = -0.49$ V vs. Fc^+/Fc) afforded a dark purple compound $[\textbf{TREN}_4Cu^{II}Cu^{II}Cu^I(\mu_3\text{-OH})](PF_6)_4$ (**4c**) in 50% yield (Figure 5A). ^{1}H NMR spectrum of **4c** show ca. 19 broad resonances from 0.13 to 122.5 ppm (Figure S8), indicating an S = 1 ground state. Complex **4c** is a rare example of a tricopper cluster with a $Cu^{II}Cu^{II}Cu^I$ oxidation state with the only other example being **2** reported by Murray *et. al.*[19] Chemical reduction of **4b** with cobaltocene (Cp_2Co, $E_{1/2} = -1.3$ V vs. Fc^+/Fc) led to a rapid color change from blue to yellow (Figure 5B), and colorless crystals of fully reduced $[\textbf{TREN}_4Cu^ICu^ICu^I(\mu_3\text{-OH})](PF_6)_2$ (**4a**) were obtained by recrystallization. ^{1}H NMR characterization of **4a** was hampered by its low solubility. Therefore, we synthesized an analog of
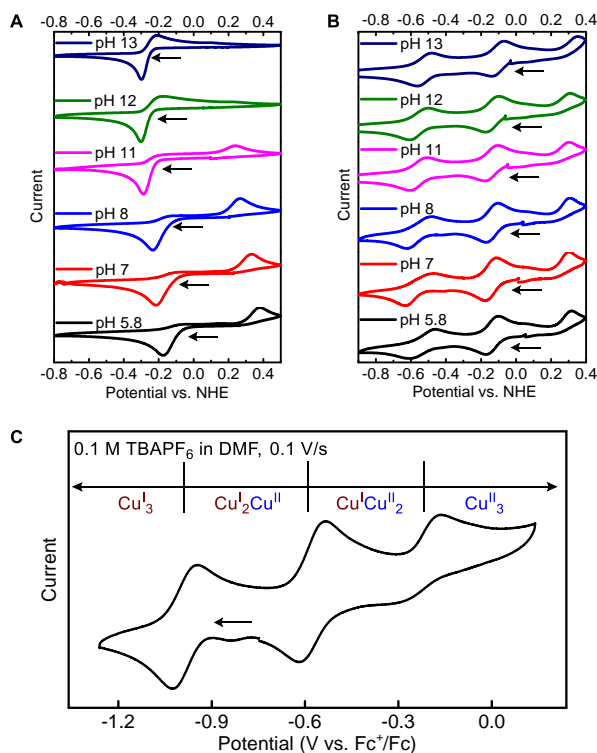
Figure 4. Cyclic voltammogram of (A) **3** and (C) **4**, in aqueous environment with various pH from 5.8 to 13 (phosphate buffer solution). (C) CV of **4** in DMF with 0.1 M (ⁿBu₄N)PF₆. Scan rate of 0.1 V/s. Working electrode: glassy carbon; counter electrode: Pt wire; reference electrode: Ag/AgNO₃.
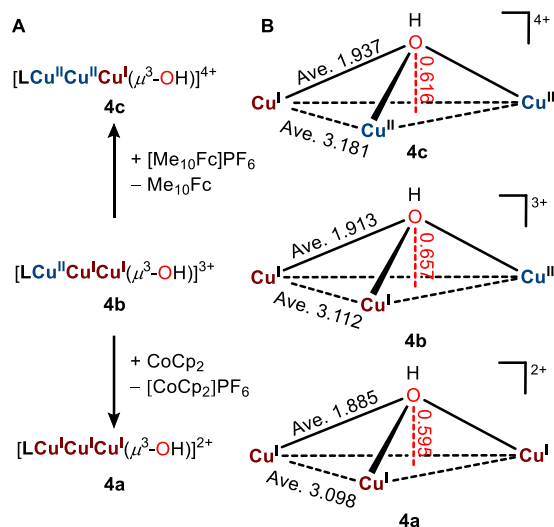
Figure 5. (A) Synthesis of **4a** and **4c** from **4b**. (B) Geometric comparison of the $Cu_3[\mu_3\text{-O(H)}]$ core in **4a**, **4b**, and **4c.** All bond metrics (Å) was determined based on X-ray single-crystal diffraction.

4a with 3,5-bis(trifluoromethyl)phenyl)borate (BAr$^F_4$) counter anions (**4a**-BAr$^F_4$) by treating **4b**-BAr$^F_4$ with Cp$_2$Co. All five ^{1}H NMR resonances of **4a**-BAr$^F_4$ between 2 to 4.5 ppm are quite broad, perhaps because of the dynamic behavior of CH$_2$ groups on **TREN$_4$** (Figure S6).

Both **4a** and **4c** were characterized by X-ray single crystallography (Figure, 5B, Figure S12-S13). The geometric features of Cu$_3$(μ_3-OH) are maintained throughout the redox processes. Complex **4a** has a slightly contracted [Cu^{I}Cu^{I}Cu^I(μ_3-OH)]$^{2+}$ core as evidenced by the shortened Cu$^{...}$Cu distance (average 3.098 Å in **4a** comparing to 3.112 Å in **4b**) and Cu-O distances (average 1.885 Å in **4a** comparing to 1.913 Å in **4b**). In contrast, the [Cu^{II}Cu^{II}Cu^I(μ_3-OH)]$^{4+}$ core in **4c** expanded (average Cu…Cu distance 3.181 Å, average Cu-O distance 1.937 Å) because of the increased Coulombic repulsion. The minimal geometric differences of complex **4a**, **4b**, and **4c** agree with their highly reversible redox behaviors. Importantly, the trigonal bipyramidal geometry of the Cu centers is preserved, even at the Cu^{I}Cu^{I}Cu^I state, highlighting the extraordinary constraints imposed by the multicyclic ligand **TREN$_4$**, a feature not shared by **TREN$_3$**.

Figure 6. (A) Infrared and (B) UV-Vis spectra of **4a** (Cu^{I}Cu^{I}Cu^I, black), **4b** (Cu^{II}Cu^{I}Cu^I, red), and **4c** (Cu^{II}Cu^{II}Cu^I, blue).

Infrared spectra of complexes **4a**, **4b**, **4c** reveal that the O-H stretches of μ_3-OH progressively blueshifts from 3372 cm^{-1} (Cu^{II}Cu^{II}Cu^I) to 3440 cm^{-1} (Cu^{II}Cu^{I}Cu^I) to 3516 cm^{-1} (Cu^{I}Cu^{I}Cu^I), in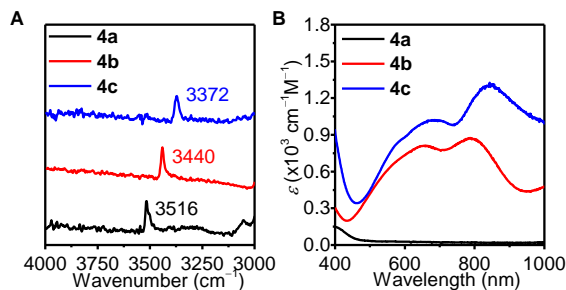dicating increasing O-H bond strength as Cu oxidation state decreases (Figure 5A). The UV-vis spectra of **4b**, **4c** both exhibit two broad intervalence charge-transfer bands (**4b**: 655 nm (800 M^{-1}cm^{-1}) and 790 nm (870 M^{-1}cm^{-1}), **4c**: 680 nm (1000 M^{-1}cm^{-1}) and 850 nm (1300 M^{-1}cm^{-1})). Time-dependent density functional theory (TD-DFT) calculations at the BP86/TZVP level showed that these absorptions originate from charge transfers from combinations of copper d orbitals to the LUMO, which features the σ* interaction of copper d_{z2} and the μ_3-O p$_z$ (Figure S22, Table S5-S6). Moreover, the calculated UV-vis spectra reflected the red-shifting trend from **4b** to **4c** (Figure S22).

Self-exchange rates (k_{11}) and reorganization energies (λ) of 4a/4b and 4b/4c. The reorganization energies (λ) of tricopper clusters during ET have important implications in oxygen reduction reaction catalyzed by MCO.[29] The reorganization energies of TNC have been used to rationalize the various rates of intermolecular ET between Type 1 Cu sites and TNC[21]

as well as the inhibition[30] or acceleration[31] of ORR by halides. To further understand the kinetic factors that govern the redox of **4**, we evaluated the self-exchange rates (k_{11}) and reorganization energy (λ) of Cu^{I}Cu^{I}Cu^I/Cu^{II}Cu^{I}Cu^I and Cu^{II}Cu^{I}Cu^I/Cu^{II}Cu^{II}Cu^I redox couples. Determine of k_{11} using ^{1}H NMR line broadening experiment[32] was not feasible due to the dynamic behavior of CH$_2$ resonances in **4a** and paramagnetic nature of **4c**. As an alternative, we employed an electrochemical method reported by Nicholson;[33,34] the self-exchange rates of **4a**/**4b** and **4b**/**4c** were determined to be 7.4(2)×10^5 M^{-1}s^{-1} and 7.2(2)×10^5 M^{-1}s^{-1}, respectively (see supporting information). These fast ET rates approach the fastest synthetic mono- and dicopper system (10^5-10^6 M^{-1}s^{-1})[33,35–39] as well as Nature's blue copper ET protein 10^5-10^6 M^{-1}s^{-1}.[40,41] The corresponding reorganization energies for **4a**/**4b** and **4b**/**4c** were calculated to be 1.21(1) eV and 1.21(1) eV using equation 1 (Z = 10^{11} M^{-1}s^{-1}, T = 298 K).[39,42]

$$k_{11} = Z\exp\left(\frac{-\lambda}{4RT}\right) \tag{1}$$

The reorganization energy (λ) can be further partitioned into inner-sphere reorganization energy (λ_i) and outersphere reorganization energy (λ_o), which are associated with structural changes of the first coordination sphere and surrounding solvents, respectively (eq 2). The outersphere reorganization energy was calculated to be 0.93 eV for **4a**/**4b** and 0.93 eV for **4b**/**4c** using eq 3, where Δe is the elementary charge, a_1 and a_2 are the radii of redox partners, and D_{opt} and D_{stat} are the optical- and static-dielectric constants of acetonitrile[43] at 298.15 K. Thus, the inner-sphere reorganization energy for **4a**/**4b** and **4b**/**4c** are estimated to be 0.28 eV and 0.28 eV using equation 2.

$$\lambda = \lambda_i + \lambda_o \tag{2}$$

$$\lambda_o = \Delta e^2\left[\frac{1}{2a_1} + \frac{1}{2a_2} - \frac{1}{a_1+a_2}\right]\left[\frac{1}{D_{opt}} - \frac{1}{D_{stat}}\right] \tag{3}$$

$$\lambda_i = \lambda_{ox} + \lambda_{red} \tag{4}$$

Determination of k_{11} of **3** was not viable, since the Cu^{II}Cu^{II}Cu^{II}/Cu^{II}Cu^{II}Cu^I was not reversible, and Cu^{II}Cu^{I}Cu^I/Cu^{I}Cu^{I}Cu^I was not observed experimentally. Therefore, we turn to computational study to compare the reorganization energy of **3** and **4**. The inner-sphere reorganization energy λ_i can be calculated by eq 4, where λ_{ox} and λ_{red} are the reorganization energy of the reduced and oxidized complexes. λ_{ox} and λ_{red} can be computationally estimated by the energy required to distort the equilibrium geometries to their redox-partners' geometries (Figure S21).[29,30,44] For example, λ_{ox} of **4a**/**4b** couple is the energy of **4b** calculated at **4a**'s optimal geometry minus the energy of **4b** at its optimal geometry. Similarly, the λ_{red} of **4a**/**4b** couple is the energy of **4a** calculated at **4b**'s optimal geometry minus the energy of **4a** at its optimal geometry (Scheme 1). The optimized geometries of **3** and **4** at all four redox states were obtained at BP86/TZVP(Cu)/SVP(H,C,N,O) level using their crystallographic structures as starting points. The reorganization energies of **3** and **4** during three ET processes (Cu^{II}Cu^{II}Cu^{II}/Cu^{II}Cu^{II}Cu^I, Cu^{II}Cu^{II}Cu^I/Cu^{II}Cu^{I}Cu^I, Cu^{II}Cu^{I}Cu^I/Cu^{I}Cu^{I}Cu^I) were summarized in Scheme 1. There are several competing spin states for the Cu^{II}Cu^{II}Cu^{II} oxidation state. Since our goal is to compare the reorganization energies of **3**

A [TREN$_4$Cu^{I}Cu^{I}Cu^{I}OH]* [TREN$_4$Cu^{II}Cu^{I}Cu^{I}OH]* [TREN$_4$Cu^{II}Cu^{II}Cu^{I}OH]* [TREN$_4$Cu^{II}Cu^{II}Cu^{II}OH]*

+ e⁻   − e⁻   + e⁻   − e⁻   + e⁻   − e⁻

λ_{red} = 0.047 eV λ_{ox} = 0.65 eV λ_{red} = 0.027 eV λ_{ox} = 0.39 eV λ_{red} = 0.13 eV λ_{ox} = 0.046 eV

[TREN$_4$Cu^{I}Cu^{I}Cu^{I}OH] [TREN$_4$Cu^{II}Cu^{I}Cu^{I}OH] [TREN$_4$Cu^{I}Cu^{II}Cu^{II}OH] [TREN$_4$Cu^{II}Cu^{II}Cu^{II}OH]

B [TREN$_3$Cu^{I}Cu^{I}Cu^{I}O]* [TREN$_3$Cu^{II}Cu^{I}Cu^{I}O]* [TREN$_3$Cu^{II}Cu^{II}Cu^{I}O]* [TREN$_3$Cu^{II}Cu^{II}Cu^{II}O]*

+ e⁻   − e⁻   + e⁻   − e⁻   + e⁻   − e⁻

λ_{red} = 1.1 eV λ_{ox} = 0.95 eV λ_{red} = 0.15 eV λ_{ox} = 0.53 eV λ_{red} = 0.084 eV λ_{ox} = 0.26 eV

[TREN$_3$Cu^{I}Cu^{I}Cu^{I}O] [TREN$_3$Cu^{II}Cu^{I}Cu^{I}O] [TREN$_3$Cu^{II}Cu^{II}Cu^{I}O] [TREN$_3$Cu^{II}Cu^{II}Cu^{II}O]

Scheme 1. Computed inner-sphere reorganization energy of (A) **4** and (B) **3**.

and **4**, we have only studied the electronic state with the lowest energies, which are the quartet states with three ferromagnetically coupled Cu(II) centers (Table S3). Complexes at Cu^{II}Cu^{II}Cu^I oxidation state were treated as triplet according to the spin state of **4c**.

The inner-sphere reorganization energies (λ_i) of **4a/4b** and **4b/4c** were well reproduced by calculations, giving confidence in the calculated λ_i in Table 1. The λ_i values for **3** and **4** differ the most for Cu^{II}Cu^{I}Cu^I/Cu^{I}Cu^{I}Cu^I redox couple (2.1 eV for **3** *vs.* 0.70 eV for **4**), consistent with the fact that the reduction of **3** to Cu^{I}Cu^{I}Cu^I state is not observed. The large inner-sphere reorganization energy for [**TREN$_3$**Cu^{II}Cu^{I}Cu^I(μ_3-O)]$^{2+}$/[**TREN$_3$**Cu^{I}Cu^{I}Cu^I(μ_3-O)]$^+$ (2.1 eV) may be rationalized by its trigonal bipyramidal Cu centers, a geometry highly preferred by Cu(II). As a result, the reduction of Cu^{II}Cu^{I}Cu^I to Cu^{I}Cu^{I}Cu^I, in an unconstrained environment, could be coupled with chemical reactions, e.g. ligand dissociation/reorganization. In contrast, multicyclic ligand **TREN$_4$** prevents such ligand dissociation and restrict solvent access to the tricopper centers, synergistically yielding small reorganization energy and fast ET rates.

Table 1. Inner-sphere reorganization energy (λ_i, *eV*) of **4** and **3**.

	Cu^{II}Cu^{I}Cu^I/ Cu^{I}Cu^{I}Cu^I	Cu^{II}Cu^{II}Cu^I/ Cu^{II}Cu^{I}Cu^I	Cu^{II}Cu^{II}Cu^{II}/ Cu^{II}Cu^{II}Cu^I
4	0.28[a]	0.28[a]	0.18[b]
	0.70[b]	0.42[b]	
3	2.1[b]	0.68[b]	0.34[b]

[a] Experimental reorganization energies determined by electrochemical measurements [b] Calculated reorganization energies by DFT.

Oxygen reduction reactivity of 4a. The generation of the fully reduced Cu^{I}Cu^{I}Cu^I state is crucial for oxygen reduction reaction at MCO. Encouraged by the redox capability of **4**, we studied its ability to reduce O$_2$. As followed by UV-Vis spectroscopy (Figure S10), fully reduced **4a** slowly reduced O$_2$,

while **4b** and **4c** did not react with O$_2$, consistent with the fact that generation of Cu^{I}Cu^{I}Cu^I state is required to harness the oxidative power of O$_2$. Addition of proton sources, e.g. acetic acid, significantly accelerated the rate of ORR. Complex **4b** was regenerated in 96(2)% spectroscopic yield. The product of the O$_2$ reduction was assigned as H$_2$O$_2$ in 97(2)% yield based on iodometric titration (see supporting information).[45] To elucidate the mechanism of ORR, we performed the reaction **4a** with ^{18}O$_2$ in the presence of acetic acid. The resulting solution of **4b** was analyzed by ESI-MS for ^{18}O incorporation. Spectrum simulations show 10% of ^{18}O incorporation, indicating that the ORR mostly likely proceeds through an outer-sphere mechanism,[46] consistent with the predominant H$_2$O$_2$ selectivity.

SUMMARY AND CONCLUSIONS

In conclusion, we report that the encapsulation of tricopper core in a protein-like cavitand activates allows the redox of three Cu^{II}/Cu^I to be harnessed effectively in a homogeneous synthetic system. The tricopper complex was isolated and characterized in three of four oxidation states, showing that the redox-induced geometric changes were minimal. The encapsulated tricopper complex has self-exchange ET rates of 10^5 – 10^6 M^{-1}s^{-1}, approaching Nature's copper electron transfer sites (blue copper protein 10^5-10^6 M^{-1}s^{-1}). Marcus analysis indicates that the reorganization energy required for the reduction of **4b** to **4a** was 0.70 eV, much smaller than that for solvent-exposed **3** (2.1 eV). These results are particularly consistent with the minimal structural difference of **4** at Cu^{I}Cu^{I}Cu^I, Cu^{II}Cu^{I}Cu^I, and Cu^{II}Cu^{II}Cu^I state and suggest that multicyclic cryptands **TREN$_4$** is effective at mimicking a protein-like environment. The geometric constraints and exclusion of solvent interactions synergistically reduce the reorganization energy of electron transfer. At last, we show that the fully reduced Cu^{I}Cu^{I}Cu^I state can participate in oxygen reduction reaction, mimicking Nature's multicopper oxidases. Taken together, our work provides insights into Nature strategy in leveraging the cooperativity of multimetallic sties in multielectron transformation – redox processes that are not operational in bulk solution could potentially be accomplished by full encapsulation of the active site in an isolated environment.

ASSOCIATED CONTENT

The Supporting information is available free of charge on the ACS Publications website at DOI:.
Experimental details, including characterization data, spectra, and computational procedures.

Crystallographic data for **4a** (CIF: 1984893)
Crystallographic data for **4b** (CIF: 1984894)
Crystallographic data for **4c** (CIF: 1984895)
Crystallographic data for **4a**-BAr$^F_4$ (CIF: 1987932)

AUTHOR INFORMATION

Corresponding Author

*zhang.8941@osu.edu

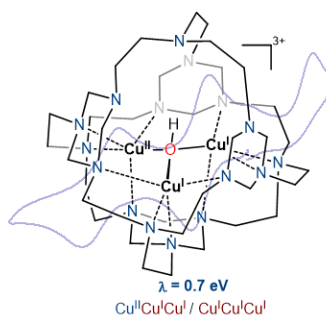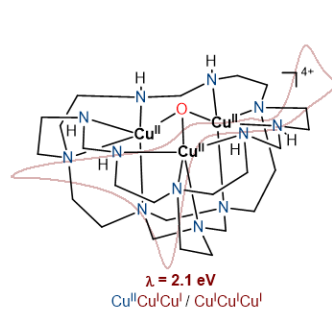### Notes

The authors declare no competing financial interest.

ACKNOWLEDGMENT

REFERENCES

(1) Gupta, A. K.; Tolman, W. B. Cu(I)/O$_2$ Chemistry Using a β-Diketiminate Supporting Ligand Derived from N,N-Dimethylhydrazine: A [Cu$_2$O$_2$]$^{3+}$ Complex with Novel Reactivity. *Inorg. Chem.* **2012**, *51*, 1881.

(2) Cole, A. P.; Root, D. E.; Mukherjee, P.; Solomon, E. I.; Stack, T. D. P. A Trinuclear Intermediate in the Copper-Mediated Reduction of O$_2$: Four Electrons from Three Coppers. *Science* **1996**, *273*, 1848.

(3) Taki, M.; Teramae, S.; Nagatomo, S.; Tachi, Y.; Kitagawa, T.; Itoh, S.; Fukuzumi, S. Fine-Tuning of Copper(I)-Dioxygen Reactivity by 2-(2-Pyridyl)Ethylamine Bidentate Ligands. *J. Am. Chem. Soc.* **2002**, *124*, 6367.

(4) Cook, B. J.; Di Francesco, G. N.; Kieber-Emmons, M. T.; Murray, L. J. A Tricopper(I) Complex Competent for O Atom Transfer, C–H Bond Activation, and Multiple O$_2$ Activation Steps. *Inorg. Chem.* **2018**, *57*, 11361.

(5) Lionetti, D.; Day, M. W.; Agapie, T. Metal-Templated Ligand Architectures for Trinuclear Chemistry: Tricopper Complexes and Their O$_2$ Reactivity. *Chem. Sci.* **2013**, *4*, 785.

(6) Engelmann, X.; Farquhar, E. R.; England, J.; Ray, K. Four-Electron Reduction of Dioxygen to Water by a Trinuclear Copper Complex. *Inorganica Chim. Acta* **2018**, *481*, 159.

(7) Tsui, E. Y.; Day, M. W.; Agapie, T. Trinucleating Copper: Synthesis and Magnetostructural Characterization of Complexes Supported by a Hexapyridyl 1,3,5-Triarylbenzene Ligand. *Angew. Chemie - Int. Ed.* **2011**, *50*, 1668.

(8) Karlin, K. D.; Qingfen, G.; Farooq, A.; Shuncheng, L.; Zubieta, J. Synthesis and X-Ray Crystal Structure of a Trinuclear Copper(I) Cluster. *Inorganica Chim. Acta* **1989**, *165*, 37.

(9) Brown, E. C.; Johnson, B.; Palavicini, S.; Kucera, B. E.; Casella, L.; Tolman, W. B. Modular Syntheses of Multidentate Ligands with Variable N-Donors: Applications to Tri- and Tetracopper(I) Complexes. *Dalt. Trans.* **2007**, No. 28, 3035.

(10) Solomon, E. I.; Sundaram, U. M.; Machonkin, T. E. Multicopper Oxidases and Oxygenases. *Chem. Rev.* **2002**, *96*, 2563.

(11) Mano, N.; Kim, H.-H.; Heller, A. On the Relationship between the Characteristics of Bilirubin Oxidases and O$_2$ Cathodes Based on Their "Wiring." *J. Phys. Chem. B* **2002**, *106*, 8842.

(12) Wang, V. C.-C.; Maji, S.; Chen, P. P.-Y.; Lee, H. K.; Yu, S. S.-F.; Chan, S. I. Alkane Oxidation: Methane Monooxygenases, Related Enzymes, and Their Biomimetics. *Chem. Rev.* **2017**, *117*, 8574.

(13) Chen, P. P.-Y.; Yang, R. B.-G.; Lee, J. C.-M.; Chan, S. I. Facile O-Atom Insertion into C-C and C-H Bonds by a Trinuclear Copper Complex Designed to Harness a Singlet Oxene. *Proc. Natl. Acad. Sci. U. S. A.* **2007**, *104*, 14570.

(14) Chan, S. I.; Lu, Y.-J.; Nagababu, P.; Maji, S.; Hung, M.-C.; Lee, M. M.; Hsu, I.-J.; Minh, P. D.; Lai, J. C.-H.; Ng, K. Y.; et al. Efficient Oxidation of Methane to Methanol by Dioxygen Mediated by Tricopper Clusters. *Angew. Chemie Int. Ed.* **2013**, *52*, 3731.

(15) Yoon, J.; Solomon, E. I. Electronic Structures of Exchange Coupled Trigonal Trimeric Cu(II) Complexes : Spin Frustration, Antisymmetric Exchange, Pseudo-A Terms, and Their Relation to O$_2$ Activation in the Multicopper Oxidases. *Coord. Chem. Rev.* **2007**, *251*, 379.

(16) Salvadeo, E.; Dubois, L.; Latour, J. Trinuclear Copper Complexes as Biological Mimics : Ligand Designs and Reactivities. *Coord. Chem. Rev.* **2018**, *374*, 345.

(17) Marcus, R. A. On the Theory of Oxidation-reduction Reactions Involving Electron Transfer. I. *J. Chem. Phys.* **1956**, *24*, 966.

(18) Rivera-carrillo, M.; Chakraborty, I.; Mezei, G.; Webster, R. D.; Raptis, R. G. Tuning of the [Cu$_3$(μ-O)]$^{4+/5+}$ Redox Couple : Spectroscopic Evidence of Charge Delocalization in the Mixed-Valent [Cu$_3$(μ-O)]$^{5+}$ Species. *Inorg. Chem.* **2008**, *47*, 7644.

(19) Cook, B. J.; Francesco, G. N. Di; Ferreira, R. B.; Lukens, J. T.; Silberstein, K. E.; Keegan, B. C.; Catalano, V. J.; Lancaster, K. M.; Shearer, J.; Murray, L. J. Chalcogen Impact on Covalency within Molecular [Cu$_3$(μ$_3$-E)]$^{3+}$ Clusters (E = O, S, Se): A Synthetic, Spectroscopic, and Computational Study. *Inorg. Chem.* **2018**, *57*, 11382.

(20) Jones, S. M.; Solomon, E. I. Electron Transfer and Reaction Mechanism of Laccases. *Cell. Mol. Life Sci.* **2015**, *72*, 869.

(21) Heppner, D. E.; Kjaergaard, C. H.; Solomon, E. I. Molecular Origin of Rapid versus Slow Intramolecular Electron Transfer in the Catalytic Cycle of the Multicopper Oxidases. *J. Am. Chem. Soc.* **2013**, *135*, 12212.

(22) Suh, M. P.; Han, M. Y.; Lee, J. H.; Min, K. S.; Hyeon, C. One-Pot Template Synthesis and Properties of a Molecular Bowl: Dodecaaza Macrotetracycle with μ$_3$-Oxo and μ$_3$-Hydroxo Tricopper (II) Cores. *J. Am. Chem. Soc.* **1998**, *120*, 3819.

(23) Yoon, J.; Mirica, L. M.; Stack, T. D. P.; Solomon, E. I. Variable-Temperature, Variable-Field Magnetic Circular Dichroism Studies of Tris-Hydroxy- and μ$_3$-Oxo-Bridged Trinuclear Cu(II) Complexes: Evaluation of Proposed Structures of the Native Intermediate of the Multicopper Oxidases. *J. Am. Chem. Soc.* **2005**, *127*, 13680.

(24) Yoon, J.; Solomon, E. I. Ground-State Electronic and Magnetic Properties of a μ$_3$-Oxo-Bridged Trinuclear Cu(II) Complex: Correlation to the Native Intermediate of the Multicopper Oxidases. *Inorg. Chem.* **2005**, *44*, 8076.

(25) Bing-guang, Z.; Hong, M.; Chun-ying, D.; Cheng, H.; Qing-jin, M.; Zhe-ming, W.; Chun-hua, Y. Novel Highly Symmetrical Cube-Shaped Cation with 16-Nitrogen Donors. *Chem. Commun.* **2001**, *24*, 2652.

(26) Garribba, E.; Micera, G. The Determination of the Geometry of Cu (II) Complexes An EPR Spectroscopy Experiment. *J. Chem. Educ.* **2006**, *83*, 1229.

(27) Kjaergaard, C. H.; Jones, S. M.; Mano, N.; Solomon, E. I. Two-Electron Reduction versus One-Electron Oxidation of the Type 3 Pair in the Multicopper Oxidases. *J. Am. Chem. Soc.* **2015**, *137*, 8783.

(28) Kjaergaard, C. H.; Durand, F.; Tasca, F.; Qayyum, M. F.; Kauffmann, B.; Gounel, S.; Suraniti, E.; Hodgson, K. O.; Hedman, B.; Mano, N.; et al. Spectroscopic and Crystallographic Characterization of "Alternative Resting" and

"Resting Oxidized" Enzyme Forms of Bilirubin Oxidase: Implications for Activity and Electrochemical Behavior of Multicopper Oxidases. *J. Am. Chem. Soc.* **2012**, *134*, 5548.

(29)   Hu, L.; Farrokhnia, M.; Heimdal, J.; Shleev, S.; Rulíšek, L.; Ryde, U. Reorganization Energy for Internal Electron Transfer in Multicopper Oxidases. *J. Phys. Chem. B* **2011**, *115*, 13111.

(30)   Kepp, K. P. Halide Binding and Inhibition of Laccase Copper Clusters: The Role of Reorganization Energy. *Inorg. Chem.* **2015**, *54*, 476.

(31)   Tian, S.; Jones, S. M.; Jose, A.; Solomon, E. I. Chloride Control of the Mechanism of Human Serum Ceruloplasmin (Cp) Catalysis. *J. Am. Chem. Soc.* **2019**, *141*, 10736.

(32)   Dahl, E. W.; Szymczak, N. K. Hydrogen Bonds Dictate the Coordination Geometry of Copper: Characterization of a Square-Planar Copper (I) Complex. *Angew. Chemie* **2016**, *128*, 3153.

(33)   Gennari, M.; Pécaut, J.; DeBeer, S.; Neese, F.; Collomb, M.-N.; Duboc, C. A Fully Delocalized Mixed-Valence Bis-µ(Thiolato) Dicopper Complex: A Structural and Functional Model of the Biological CuA Center. *Angew. Chemie Int. Ed.* **2011**, *50*, 5662.

(34)   Nicholson, R. S. Theory and Application of Cyclic Voltammetry for Measurement of Electrode Reaction Kinetics. *Anal. Chem.* **1965**, *37*, 1351.

(35)   Dahl, E. W.; Szymczak, N. K. Hydrogen Bonds Dictate the Coordination Geometry of Copper: Characterization of a Square-Planar Copper(I) Complex. *Angew. Chemie Int. Ed.* **2016**, *128*, 3153.

(36)   Doine, H.; Yano, Y.; Swaddle, T. W. Kinetics of the Bis(2,9-Dimethyl-1,10-Phenanthroline)Copper(I/II) Self Exchange Reaction in Solution. *Inorg. Chem.* **1989**, *28*, 2319.

(37)   Krylova, K.; Kulatilleke, C. P.; Heeg, M. J.; Salhi, C. A.; Ochrymowycz, L. A.; Rorabacher, D. B. A Structural Strategy for Generating Rapid Electron-Transfer Kinetics in Copper(II/I) Systems. *Inorg. Chem.* **1999**, *38*, 4322.

(38)   Pulliam, E. J.; McMillin, D. R. Self-Exchange Rate for the Copper(II)/Copper(I) Couple Complexed to TAAB, an N_4 Macrocycle. *Inorg. Chem.* **1984**, *23*, 1172.

(39)   Zerk, T. J.; Saouma, C. T.; Mayer, J. M.; Tolman, W. B. Low Reorganization Energy for Electron Self-Exchange by a Formally Copper(III,II) Redox Couple. *Inorg. Chem.* **2019**, *58*, 14151.

(40)   Slutter, C. E.; Langen, R.; Sanders, D.; Lawrence, S. M.; Wittung, P.; Di Bilio, A. J.; Hill, M. G.; Fee, J. A.; Richards, J. H.; Winkler, J. R.; et al. Electron-Transfer Studies with the CuA Domain of Thermus Thermophilus Cytochrome Ba3. *Inorganica Chim. Acta* **1996**, *243*, 141.

(41)   Adman, E. T.; Canters, G. W.; Hill, H. A. O.; Kitchen, N. A. The Redox Properties of Azurin from Pseudomonas Aeruginosa as Studied by High Frequency Proton NMR. *Inorganica Chim. Acta* **1983**, *79*, 127.

(42)   Eberson, L. E. *Electron Transfer Reactions in Organic Chemistry*; Springer-Verlag: Berlin, 1987.

(43)   Moreau, C.; Gérard, D. Thermodynamic and Physical Behaviour of Water + Acetonitrile Mixtures. Dielectric Properties. *J. Chem. Thermodyn.* **1976**, *8*, 403.

(44)   Sigfridsson, E.; Olsson, M. H. M.; Ryde, U. Inner-Sphere Reorganization Energy of Iron−Sulfur Clusters Studied with Theoretical Methods. *Inorg. Chem.* **2001**, *40*, 2509.

(45)   Garcia-bosch, I.; Cowley, R. E.; Díaz, D. E.; Siegler, M. A.; Nam, W.; Solomon, E. I.; Karlin, K. D. Dioxygen Activation by a Macrocyclic Copper Complex Leads to a Cu_2O_2 Core with Unexpected Structure and Reactivity. *Chem. – A Eur. J.* **2016**, *22*, 5133.

(46)   Pegis, M. L.; Wise, C. F.; Martin, D. J.; Mayer, J. M. Oxygen Reduction by Homogeneous Molecular Catalysts and Electrocatalysts. *Chem. Rev.* **2018**, *118*, 2340.

λ = 2.1 eV
$Cu^{II}Cu^{I}Cu^{I}$ / $Cu^{I}Cu^{I}Cu^{I}$

λ = 0.7 eV
$Cu^{II}Cu^{I}Cu^{I}$ / $Cu^{I}Cu^{I}Cu^{I}$

Electronic Supporting Information for:

Encapsulation of synthetic tricopper cluster in a protein-like cavitand enables facile redox processes from $Cu^{I}Cu^{I}Cu^{I}$ to $Cu^{II}Cu^{II}Cu^{II}$ states

Weiyao Zhang, Curtis E. Moore, Shiyu Zhang[*]

Department of Chemistry and Biochemistry, The Ohio State University, 100 West 18th Avenue, Columbus, Ohio 43210, United States

Contents

1.Materials and Methods

General: All reactions were carried out under a nitrogen atmosphere in an MBraun glovebox or using Schlenk techniques.

Instrumentation: Nuclear magnetic resonance (NMR) spectra were recorded on DXP 400 MHz (^{1}H: 400 MHz) and AVIII 600 MHz (^{1}H: 600 MHz) at ambient temperature. Chemical shift values for protons were referenced to the residual proton resonance of acetone-d_6 (δ: 2.05 ppm) and tetrahydrofuran-d_8 (THF-d_8, δ: 1.72 ppm and 3.58 ppm). X-ray crystallographic analyses were performed under a cold nitrogen stream (Oxford Cryosystems Cryostream) at 100 K (**4a, 4b, 4c, 4a**-BAr$^F_4$) on a Bruker D8 Venture instrument with Mo Ka ra-

diation source ($\lambda = 0.7107$ Å) and a Photon II detector. Elemental analyses were performed by Midwest Micro Lab (Indianapolis, IN, http://midwestlab.com/). ESI mass spectra were recorded on a Bruker MicrOTOF. EPR measurements were performed in 4 mm low-pressure quartz tubes on a Bruker EMXPlus X-band EPR spectrometer equipped with a Coldedge cryostat with small-volume power saturation. Solid-state IR was recorded on a Bruker Alpha II FTIR spectrometer. Cyclic voltammogram was performed using Bio-Logic SAS SP-50 with a glassy carbon working electrode, a platinum wire counter electrode and a Ag/Ag^+ reference electrode (a commercial leakless miniature Ag/AgCl reference is used for aqueous solution and a $Ag/AgNO_3$ (0.01 M) reference electrode is used for organic solution).

Materials: Anhydrous acetone and anhydrous methanol were purchased from Acros and Alfa Aesar, respectively, and were used as received. Dichloromethane, acetonitrile, diethyl ether, tetrahydrofuran, and fluorobenzene were dried and degassed under nitrogen using a Pure Process Technologies (PPT, Nashua, NH) solvent purification system, and stored over 4 Å molecular sieves. Acetone-d_6 (Cambridge Isotope Laboratories, Inc.) was purified by distillation, deoxygenated by three freeze-pump-thaw cycles, and dried over 4 Å molecular sieves prior to use. Tetrahydrofuran-d_8 (Cambridge Isotope Laboratories, Inc.) was deoxygenated by three freeze-pump-thaw cycles and dried over 4 Å molecular sieves prior to use. Tetrakis(acetonitrile)copper(I) hexafluorophosphate (Sigma-Aldrich), paraformaldehyde (Acros), tris(2-aminoethyl) amine (TREN, TCI), cobaltocene (Strem), tetra-n-butylammonium tetrafluoroborate (Sigma-Aldrich), tetra-n-butylammonium chloride (Combi-Blocks), decamethylferrocene (Sigma-Aldrich), silver hexafluorophosphate (Strem), iodine (VWR), sodium iodide (Sigma-Aldrich), triazabicyclodecene (TBD, Sigma-Aldrich), dioxygen (Praxair), and ^{18}O-dioxygen (Sigma-Aldrich) were purchased and used without further purification. Sodium tetrakis[(3,5-trifluoromethyl)phenyl]borate was prepared by a published method.[1] AcOH (glacial, Fisher) and heptane (anhydrous, Alfa Aesar) were deoxygenated by three freeze-pump-thaw cycles before use.

Synthesis and characterization of [TREN$_4$Cu^{I}Cu^{I}Cu^{II}(μ_3-OH)](PF$_6$)$_3$ (4b)

$$TREN + Cu(MeCN)_4PF_6 + paraformaldehyde \xrightarrow[\text{80 °C, two days}]{\text{MeCN, N}_2} \textbf{[TREN}_4Cu^{II}Cu^ICu^I(\mu_3\text{-OH}](PF_6)_3$$

Yield: 18%
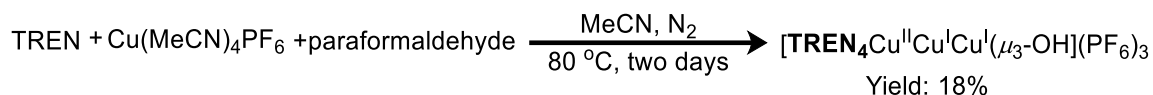
Tetrakis(acetonitrile)copper(I) hexafluorophosphate (93.3 mg, 0.251 mmol), paraformaldehyde (150 mg, 50.0 mmol), and acetonitrile (10 mL) were added to a 20 mL scintillation vial equipped with a septum under nitrogen atmosphere. Tris(2-aminoethyl) amine (TREN, 0.150 mL, 1.00 mmol) was injected with a syringe. Four other vials with the same suspension were prepared in parallel. The five vials were sealed and heated at 80 °C with vigorous stirring for two days, during which the solution turned dark brown. After the reaction, the solution was allowed to cool down and transferred back to the glovebox. The dark brown suspension from five vials was combined and filtered under a nitrogen atmosphere. The brown filtrate was dried under vacuum to afford an orange oil-like residue. Dichloromethane (10 mL) was added to the residue, and the resulting suspension was allowed to sit overnight at room temperature to yield a mixture of a blue solid and a yellow solid, which was collected by filtration and washed with additional dichloromethane (*ca.* 10 mL), and extracted into acetone (15 mL). The acetone solution was filtered, and all volatiles were removed under vacuum to yield a blue solid. The product was rewashed with dichloromethane (*ca.* 10 mL) and dried under vacuum to afford 106.8 mg of **4b** (18% yield). Single crystals of **4b** suitable for X-ray diffraction were obtained by diffusing diethyl ether to an acetone solution of **4b** at −30 °C.
Elemental analysis, Calcd for $C_{36}H_{73}Cu_3F_{18}N_{16}OP_3$ C, 31.52; H, 5.36; N, 16.34. found C, 31.75; H, 5.39; N, 16.06.
Infrared spectrum (ATR), $\nu OH = 3440$ cm^{-1} (Figure 6);
UV-Vis spectrum (acetone, Figure S1), $\lambda_{max} = 655$ nm (800 M^{-1}cm^{-1}), 790 nm (870 M^{-1}cm^{-1});

ESI-MS spectrum (Figure S2), M/z = 312.2;
EPR spectrum (acetonitrile, 50 K, Figure S16), $g_1 = 2.14$, $g_2 = 2.25$, $g_3 = 2.01$, $A_3 = 146$ MHz.
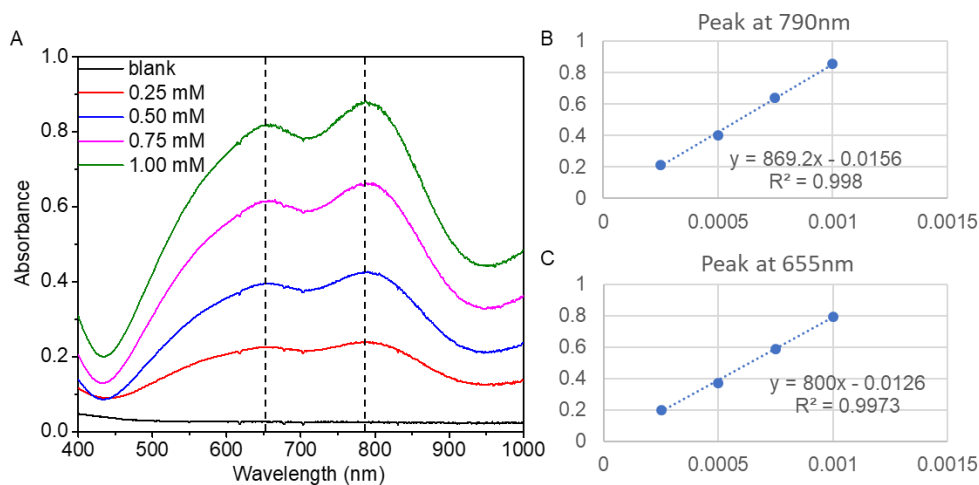
Figure S1. (A) UV-Vis spectra of [**TREN**$_4$Cu^{I}Cu^{I}Cu^{II}(μ_3-OH)](PF$_6$)$_3$ (**4b**) at various concentration in acetone at room temperature; Beer's law plots for the peak at 790 nm (B, $\varepsilon = 870$ M^{-1}cm^{-1}) and 655 nm (C, $\varepsilon = 800$ M^{-1}cm^{-1}).
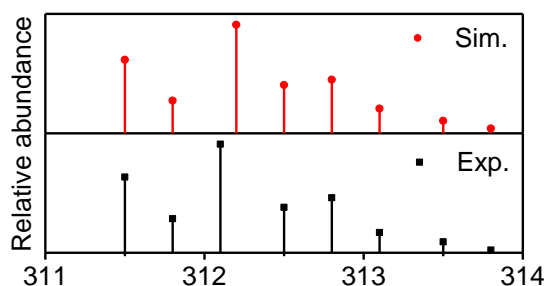
Figure S2. ESI-MS spectrum (MeCN) and simulation of [**TREN**$_4$Cu^{I}Cu^{I}Cu^{II}(μ_3-OH)](PF$_6$)$_3$.

Synthesis and characterization of [TREN$_4$Cu^{I}Cu^{I}Cu^{II}(μ_3-OH)](BAr$^F_4$)$_3$ (4b-BAr$^F_4$)
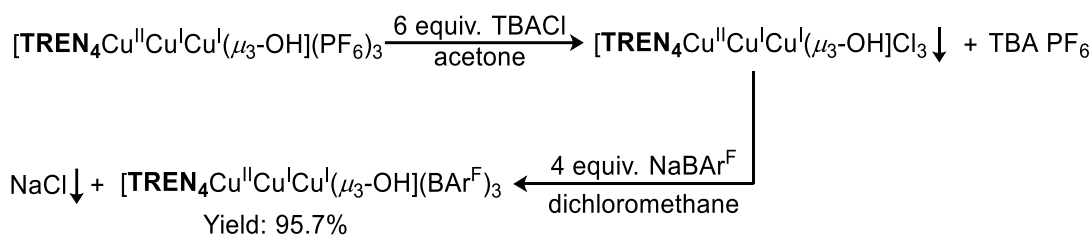
To an acetone (1 mL) solution of tetra-n-butylammonium chloride (60.8 mg, 0.219 mmol), an acetone (4 mL) solution of [**TREN**$_4$Cu^{I}Cu^{I}Cu^{II}(μ_3-OH)](PF$_6$)$_3$ (40.0 mg, 0.0292 mmol) was added dropwise with stirring. A blue precipitate was formed immediately and collected by filtration. After being washed by acetone (ca. 2 mL), the blue solid was dried under vacuum. Then, a dichloromethane (3 mL) suspension of the obtained blue solid was added to a dichloromethane (2 mL) suspension of sodium tetrakis[(3,5-trifluoromethyl)phenyl]borate (103.5 mg, 0.117 mmol). The mixture was allowed to stir at room temperature overnight. After filtration, the blue filtrate was collected and dried under vacuum. The obtained blue solid was washed with diethyl ether (*ca.* 3 mL, three times) and dried under vacuum to afford the desired product **4b**-BAr$^F_4$ (98.3 mg, 96% yield).
Elemental analysis, Calcd for C$_{132}$H$_{109}$B$_3$Cu$_3$F$_{72}$N$_{16}$O C, 44.96; H, 3.12; N, 6.36. found C,

44.65; H, 3.19; N, 6.23.

Synthesis and characterization of [TREN$_4$Cu^{I}Cu^{I}Cu^I(μ_3-OH)](PF$_6$)$_2$ (4a)

$$[\textbf{TREN}_4\text{Cu}^{II}\text{Cu}^I\text{Cu}^I(\mu_3\text{-OH})](\text{PF}_6)_3 + \text{Cp}_2\text{Co} \xrightarrow[\text{room temperature}]{\text{acetone, N}_2} [\textbf{TREN}_4\text{Cu}^I\text{Cu}^I\text{Cu}^I(\mu_3\text{-OH})](\text{PF}_6)_2$$

Yield: 19%
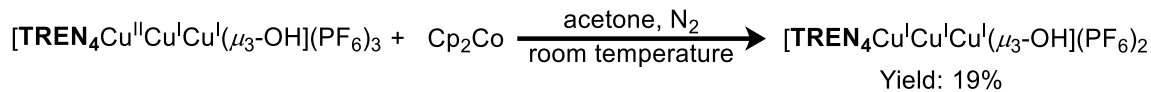
To an acetone (6 mL) solution of [**TREN**$_4$Cu^{I}Cu^{I}Cu^{II}(μ_3-OH)](PF$_6$)$_3$ (**4b**, 40.0 mg, 0.0292 mmol), an acetone (2 mL) solution of CoCp$_2$ (6.1 mg, and 0.0321 mmol, 1.1 eq) was added under nitrogen atmosphere. The mixture was stirred at room temperature for five minutes, during which the color of the solution turns yellow. All volatiles were removed under vacuum, and the yielded yellow residue was washed by THF (*ca.*15 mL). After dried under vacuum, the solid was dissolved in acetone (*ca.* 1.5 ml). Slow diffusion of diethyl ether to the acetone solution at −30 ºC afford colorless crystals of **4a** (6.7 mg, yield 19%) suitable for XRD (Figure S11). ^{1}H NMR analysis of the crystals (Figure S3) shows a mixture of **4a** (marked with blue dots) and a small amount of impurity that appears to be the protonated species [**4a**+H] with sharp resonances at 9.20, 4.34, 3.30, 2.72, 2.45, and 2.36 ppm (marked with red dots, Figure S3). We believe that the protonation of **4a** was due to the residual water in acetone-d_6, which cannot be completely removed without causing the decomposition of acetone-d_6. Unfortunately, we were unable to obtain a solution of **4a** in THF-d_8 due to its low solubility. Other NMR solvents, e.g. acetonitrile-d_3, cause rapid decomposition of **4a** back to **4b**. To confirm these sharp resonances (9.20, 4.34, 3.30, 2.72, 2.45, and 2.36 ppm) are from protonated **4a**, we prepared the BAr$^F_4$ analog **4a**-BAr$^F_4$, which can be dissolved and analyzed in THF-d_8 (*infra vide*).

Infrared spectrum, νOH = 3516 cm^{-1} (Figure 6).
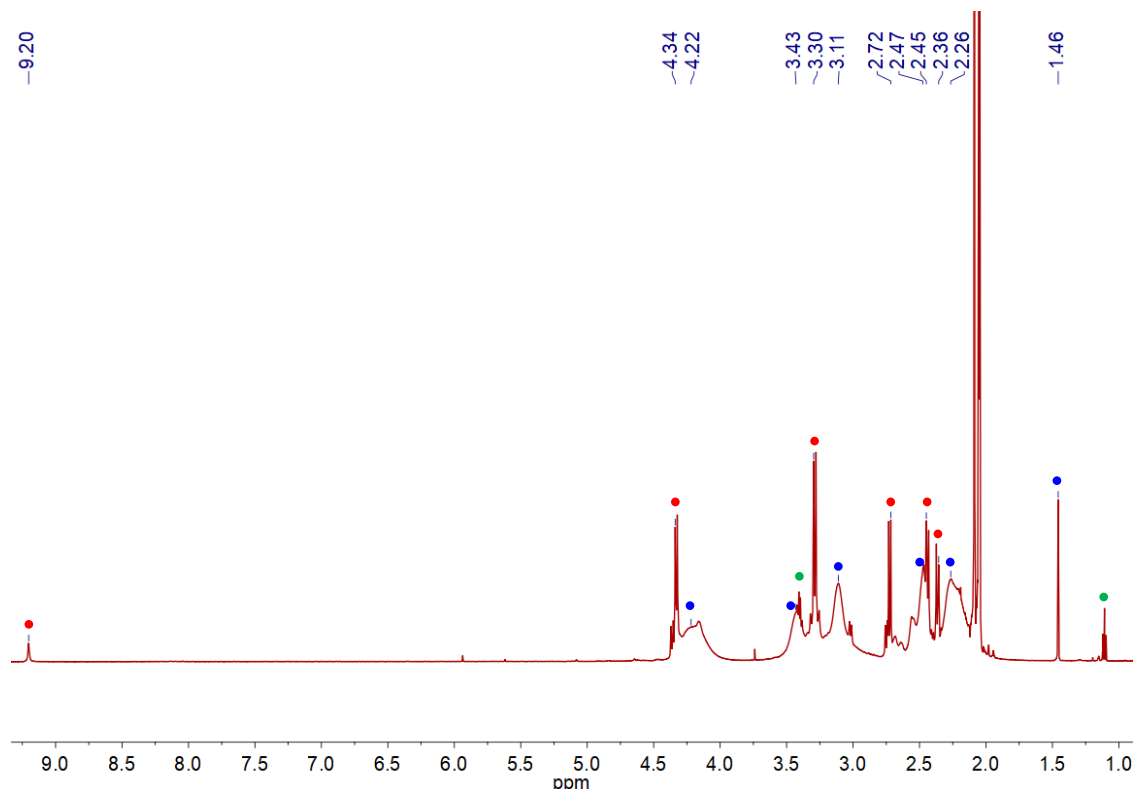
Figure S3. ^{1}H NMR spectrum (600 MHz, acetone-d_6) of **4a** (blue dots). The peaks marked with green dots are from residual diethyl ether. The peaks marked with red dots are from protonated **4a**.
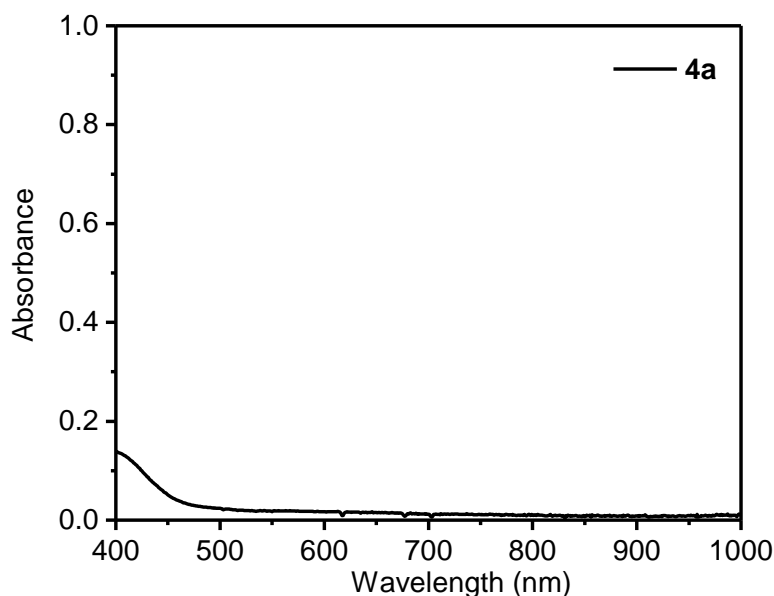
Figure S4. UV-Vis spectrum of [**TREN₄**Cu^{I}Cu^{I}Cu^I(μ_3-OH)](PF$_6$)$_2$ (**4a**) in acetone at room temperature. The UV-Vis sample was generated in-situ from the treatment of [**TREN₄**Cu^{I}Cu^{I}Cu^{II}(μ_3-OH)](PF$_6$)$_3$ (**4b**) with one equivalent of Cp$_2$Co.
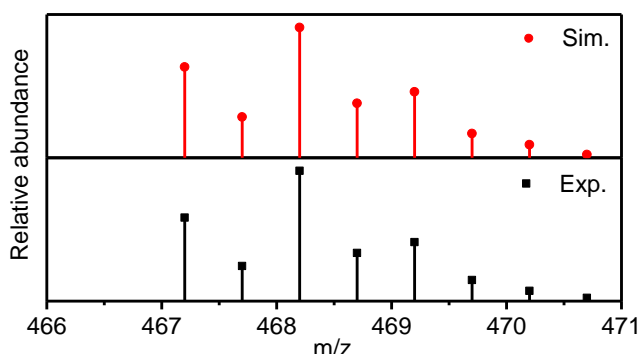
Figure S5. ESI-MS spectrum (MeCN) and simulation of [**TREN₄**Cu^{I}Cu^{I}Cu^I(μ_3-OH)](PF$_6$)$_2$ (**4a**).

Synthesis and characterization of [TREN₄Cu^{I}Cu^{I}Cu^I(μ_3-OH)](BAr$^F_4$)$_2$ (4a-BAr$^F_4$)

$$[\textbf{TREN}_4\text{Cu}^{II}\text{Cu}^I\text{Cu}^I(\mu_3\text{-OH})](\text{BAr}^F)_3 + \text{Cp}_2\text{Co} \xrightarrow[-\ [\text{Cp}_2\text{Co}]\text{BAr}^F_4]{\text{Fluorobenzene}} [\textbf{TREN}_4\text{Cu}^I\text{Cu}^I\text{Cu}^I(\mu_3\text{-OH})](\text{BAr}^F)_2$$

1 equiv.　　　　　2.4 equiv.　　　　　　　　Yield: 50.5%
　　　　　　　0.2 mL DCM solution
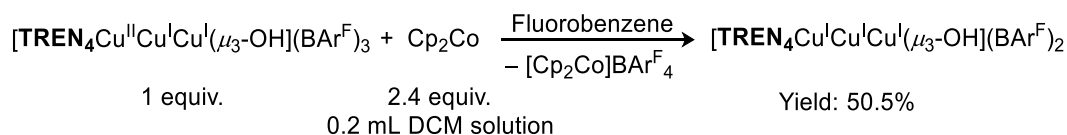
To a suspension of **4b**-BAr$^F_4$ (10.0 mg, 0.00284 mmol) in fluorobenzene (1 mL), a dichloro-methane (0.2 mL) solution of Cp$_2$Co (1.3 mg, 0.0068 mmol) was added with stirring. The blue **4b**-BAr$^F_4$ was gradually dissolved and the solution turned yellow. After filtration, the yellow filtrate was allowed to sit at room temperature overnight. Colorless needle-like crystals of **4a**-BAr$^F_4$ suitable for single-crystal X-ray diffraction were obtained. The mother liquid was pipetted out and the crystals were washed by fluorobenzene (*ca.* 5 mL) for three times. The obtained white solid was dissolved in THF (1.5 mL) and treated with triazabicyclodecene (2.0 mg, 0.014 mmol). After about one minute, the resulting suspension was filtered, and the filtrate was dried under vacuum. The obtained solid was washed with fluorobenzene (*ca.* 8 mL, five times) and dried under vacuum to afford **4a**-BAr$^F_4$ (3.8 mg, 51 % yield). (Figure

S12). ^{1}H NMR (600 MHz, THF-d_8, Figure S6) δ 7.79 (br, 16H), 7.58 (br, 8H), 3.98 (br, 12H), 3.28 (br, 12H), 2.92 (br, 12H), 2.44 (br, 12H), 2.19 (br, 24H), 1.35 (s, 1H);
Elemental analysis, Calcd for $C_{100}H_{97}B_2Cu_3F_{48}N_{16}O$ C, 45.10; H, 3.67; N, 8.42. found C, 45.17; H, 3.84; N, 8.45.
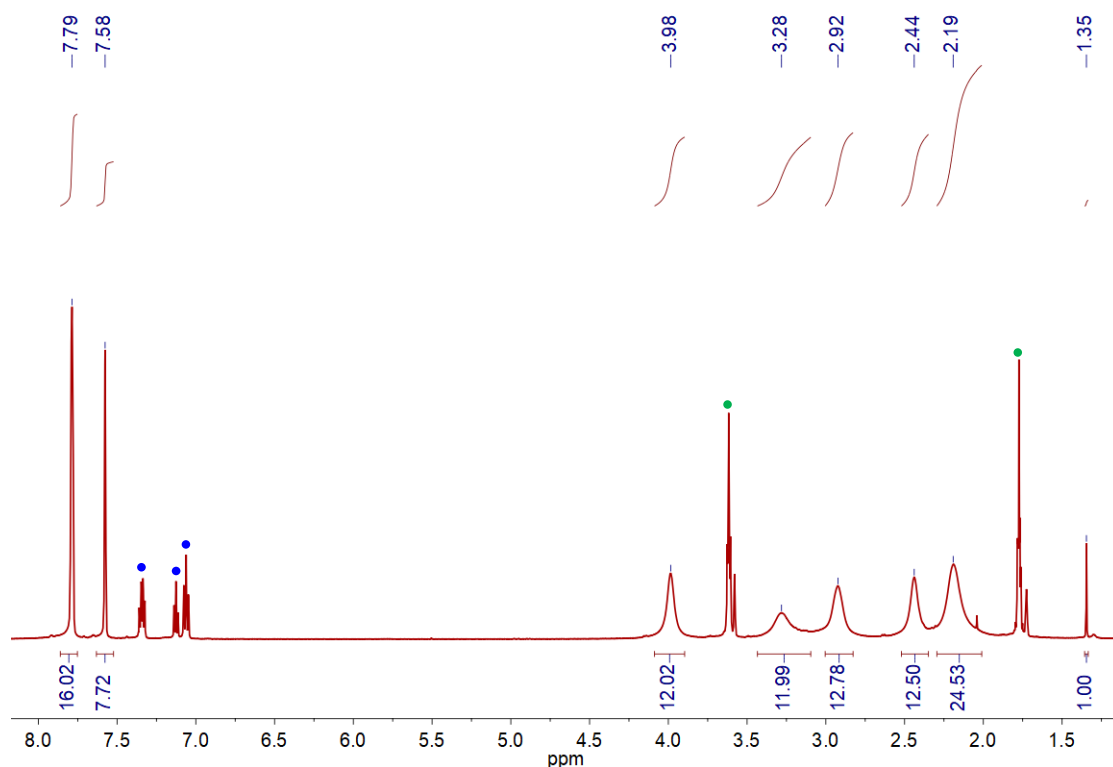
Figure S6. ^{1}H NMR spectrum (600 MHz, THF-d_8) of **4a**-BAr$^F_4$. The peaks marked with blue dots are from residual fluorobenzene. The peaks marked with green spots are from residual THF.

Synthesis and characterization of [TREN$_4$Cu^{I}Cu^{II}Cu^{II}(μ_3-OH)] (PF$_6$)$_4$ (4c)

$$[\textbf{TREN}_4Cu^{II}Cu^ICu^I(\mu_3\text{-OH})](PF_6)_3 + Me_{10}Fc^+ PF_6^- \xrightarrow[\text{room temperature}]{\text{acetone, N}_2} [\textbf{TREN}_4Cu^ICu^{II}Cu^{II}(\mu_3\text{-OH})](PF_6)_4$$

Yield: 50%
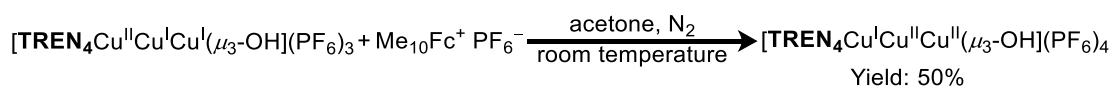
To an acetone (3 mL) solution of [**TREN**$_4$Cu^{I}Cu^{I}Cu^{II}(μ_3-OH)](PF$_6$)$_3$ (20.0 mg, 0.0140 mmol), an acetone (4 mL) solution of decamethylferrocenium hexafluorophosphate (9.4 mg, 0.020 mmol) was added under nitrogen atmosphere. The mixture was allowed to stir at room temperature for ten minutes. The solution was dried under vacuum and the yielded solid was re-dissolved in acetone (*ca.* 1 mL). THF (*ca.* 15 mL) was then added to the acetone solution with stirring. The obtained suspension was filtered and the dark blue precipitate was collected and dried under vacuum to afford **4c** (10.6 mg, 50 % yield) as a dark blue powder.
Elemental analysis, Calcd for **4c**•(CH$_3$C(O)CH$_3$)$_2$, $C_{42}H_{85}Cu_3F_{24}N_{16}OP_4$: C, 30.90; H, 5.25; N, 13.73. found C, 30.05; H, 5.26; N, 13.70.
UV-Vis spectrum (acetone, Figure S7), λ_{max} = 680 nm (970 M^{-1}cm^{-1}), 850 nm (1250 M^{-1}cm^{-1});
Infrared spectrum, νOH = 3372 cm^{-1} (Figure 6).
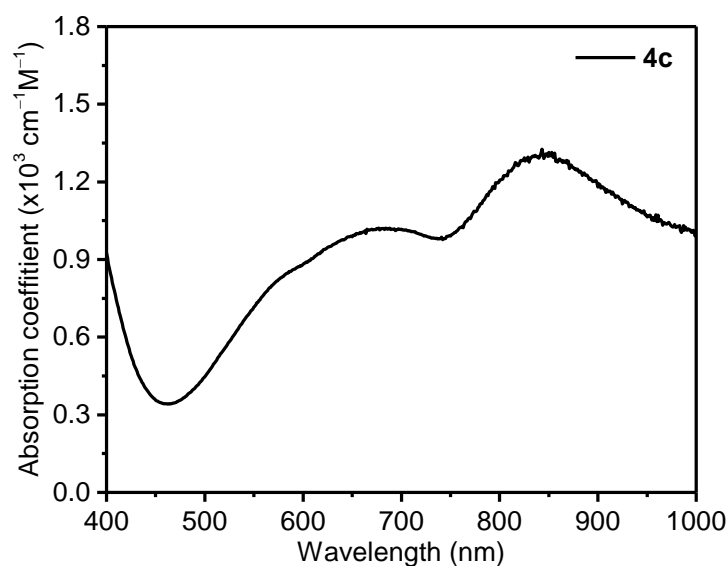
Figure S7. UV-Vis spectrum of [**TREN**$_4$Cu^{I}Cu^{II}Cu^{II}(μ_3-OH)](PF$_6$)$_4$ in acetonitrile at room temperature. Two maxima at 680 nm and 850 nm were observed.

In order to obtain crystals of [**TREN**$_4$Cu^{I}Cu^{II}Cu^{II}(μ_3-OH)]$^{4+}$ for single-crystal X-ray diffraction analysis, [**TREN**$_4$Cu^{I}Cu^{II}Cu^{II}(μ_3-OH)](PF$_6$)$_4$ (10.0 mg, 0.00659 mmol) and tetra-n-butylammonium tetrafluoroborate (TBABF$_4$, 2.0 mg, 0.0060 mmol) was dissolved in acetone (*ca.* 1 mL). Slow diffusion of diethyl ether to the mixture of [**TREN**$_4$Cu^{I}Cu^{II}Cu^{II}(μ_3-OH)](PF$_6$)$_4$ and TBABF$_4$ at − 30°C afford single crystals of [**TREN**$_4$Cu^{I}Cu^{II}Cu^{II}(μ_3-OH)](PF$_6$)(BF$_4$)$_3$ (Figure S13).
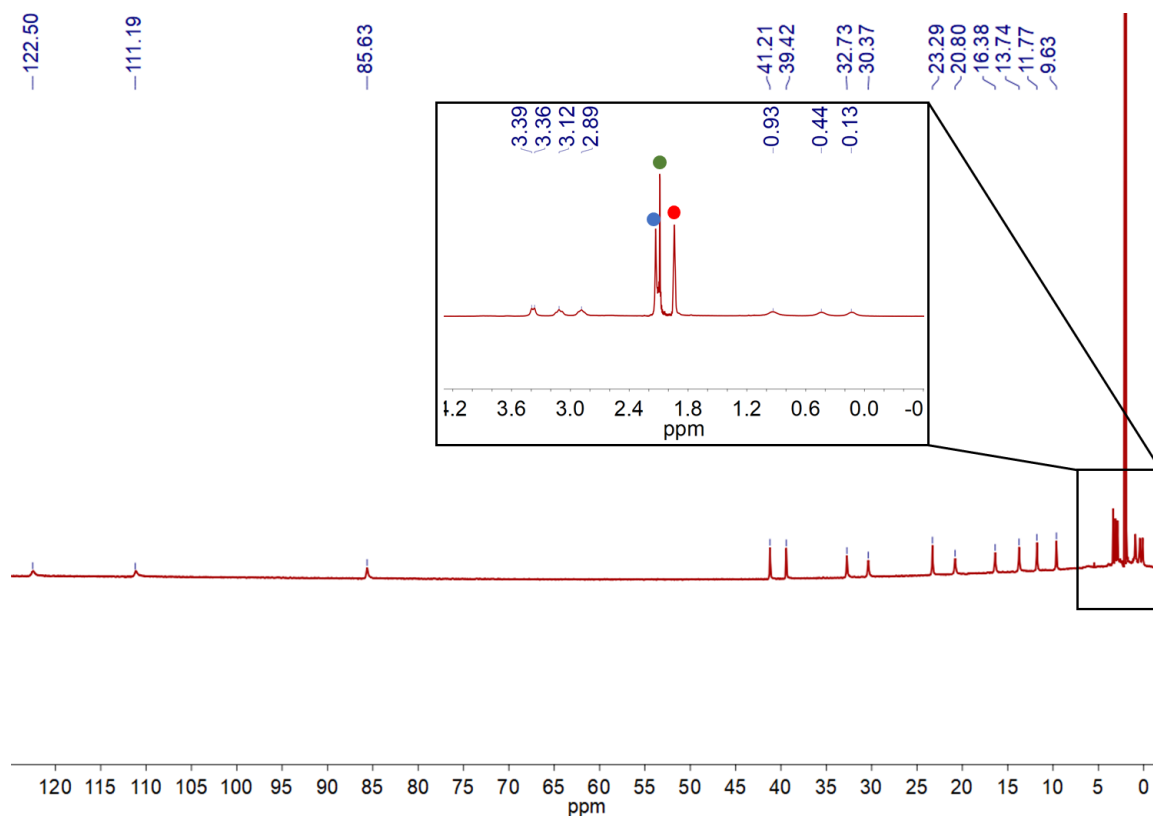
Figure S8. ^{1}H NMR (400 MHz, CD$_3$CN) spectrum of [**TREN**$_4$Cu^{I}Cu^{II}Cu^{II}(μ_3-OH)](PF$_6$)$_4$ (**4c**).

The peak marked with a red dot is from residual CD_2HCN from the NMR solvent. The peak marked with a green dot is from residual acetone. The peak marked with a green dot is from residual water.

Synthesis and characterization of decamethylferrocenium hexafluorophosphate

$$Me_{10}Fc \ + \ AgPF_6 \ \xrightarrow[\text{room temperature}]{\text{acetone, N}_2} \ Me_{10}Fc^+ \ PF_6^- \ + \ Ag$$
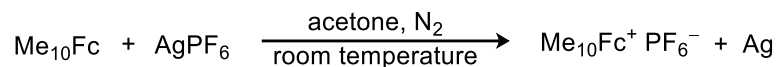
Yield: 80%

To an acetone suspension (5 mL) of decamethylferrocene (154.6 mg, 0.4738 mmol), an acetone solution (2 mL) of $AgPF_6$ (100.0 mg, 0.3955 mmol) was added dropwise with stirring. The obtained mixture was allowed to stir at room temperature for three hours. After filtration, the green filtrate was collected and dried under vacuum. The green-yellow solid was then dissolved in acetone (*ca.* 5 mL). Diethyl ether (*ca.* 15 mL) was added to the acetone solution to precipitate out the product. The green solid was collected with filtration and dried under vacuum. Block crystals of the product were obtained by diffusing diethyl ether into an acetone solution (5 mL) at room temperature overnight (149.9 mg, Yield 80.3%).

Elemental analysis, Calcd for $C_{20}H_{30}F_6FeP$ C, 50.97; H, 6.42 found C, 51.42; H, 6.38.

2. UV-Vis spectroscopy Studies Details

Determining the molar extinction coefficient of NaI$_3$ in an acetone/heptane (2:3) mixture

$$NaI + I_2 \longrightarrow NaI_3$$
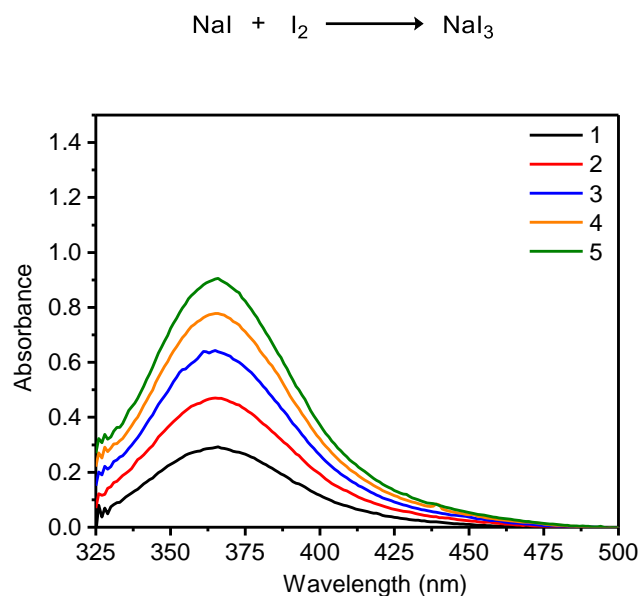
Figure S9. Solutions of NaI$_3$ with various concentrations were prepared by adding a solution of I$_2$ (0.2 mL, 1.2 mM) to NaI (2 mL, 50 mM, excess) in acetone/heptane (2:3) sequentially. The UV-Vis traces of the solutions were recorded at 0.0109 mM (trace 1), 0.0200 mM (trace 2), 0.0277 mM (trace 3), 0.0343 mM (trace 4), and 0.0400 mM (trace 5). The molar extinction coefficient of NaI$_3$ at 364 nm was calculated as 2.13×10^4 cm^{-1}M^{-1}.

Quantification of H$_2$O$_2$ produced from the reaction of 4a and O$_2$
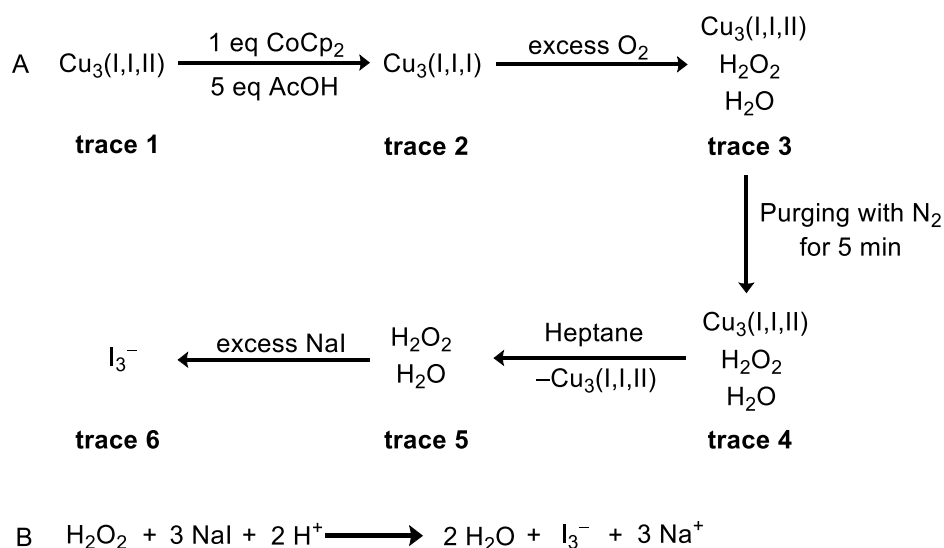
Scheme S1. (A) H$_2$O$_2$ quantification from the stoichiometric reaction between **4a** and O$_2$. (B) The reaction of H$_2$O$_2$ and NaI.

In glovebox, an acetone solution of [**TREN$_4$**Cu^{I}Cu^{I}Cu^{II}(μ_3-OH)](PF$_6$)$_3$ (**4b**, 1.4 mg, 1.0 μmol, 2.00 mL, 0.5 mM) was transferred to a Schlenk quartz cuvette. The cuvette was sealed and transferred to the UV-Vis spectrometer (Figure S9, trace 1). Under nitrogen protection, an ac-

etone solution of Cp_2Co (0.19 mg, 1.0 μmol, 0.500 mL acetone) and acetic acid (0.30 mg, 5.0 μmol, 5 equiv., 0.500 mL acetone) were injected to the cuvette. The 790 nm and 655 nm bands of complex **4b** ($Cu^{II}Cu^{I}Cu^{I}$) were bleached instantaneously (Figure S10, trace 2, Scheme 1), indicating the formation of complex **4a** ($Cu^{I}Cu^{I}Cu^{I}$). Oxygen gas (0.500 ml, 20.5 μmol, 20.5 equiv.) was injected to the cuvette (Figure S10, trace 3). The progress of oxygen reduction reaction was monitored by taking a UV-Vis spectrum every 60 seconds. Two bands at 790 nm and 655 nm grew in over 5 minutes, indicating the reformation of complex **4b** ($Cu^{II}Cu^{I}Cu^{I}$) in 96% spectroscopic yield. The solution in the Schlenk quartz cuvette was purged with N_2 for five minutes to remove the excess oxygen (Figure S10, trace 4). The cuvette was sealed and transferred back into glovebox. The solution in cuvette was transferred to a scintillation vial. The cuvette was washed with additional acetone (1 mL) to ensure complete transfer. Additional acetone (0.354 mL, calculated based on absorbance increase at 790 nm after purging) was added to the scintillation vial in order to compensate the solvent loss during the N_2 purging process. To the combined acetone solution, heptane (6 ml) was added in order to precipitate out all the copper complexes. The obtained suspension was then filtered, and the filtrate (2 mL) was transferred to a new Schlenk quartz cuvette (Figure S10, trace 5). Acetone/heptane (2:3) solution of NaI (7.5 mg, 50 μmol, 0.500 mL) was injected to the solution in the cuvette (Figure S10, trace 6). The reaction between H_2O_2 and NaI affords I_3^- (Scheme S1, B), the yield of which can be determined by its characteristic absorbance at λ_{max} = 364 nm ($\varepsilon = 2.1 \times 10^4$ M^{-1} cm^{-1}). The H_2O_2 quantification results from three independent trials are summarized in Table S1.

Entry	Experiment 1	Experiment 2	Experiment 3	average
Absorbance / I_3^-	0.817	0.813	0.847	0.826
Amount / mmol	9.57×10^{-5}	9.52×10^{-5}	9.92×10^{-5}	9.67×10^{-5}
Yield of H_2O_2	96%	95%	99%	97%

Table S1. Yields of H_2O_2 in three independent trials.
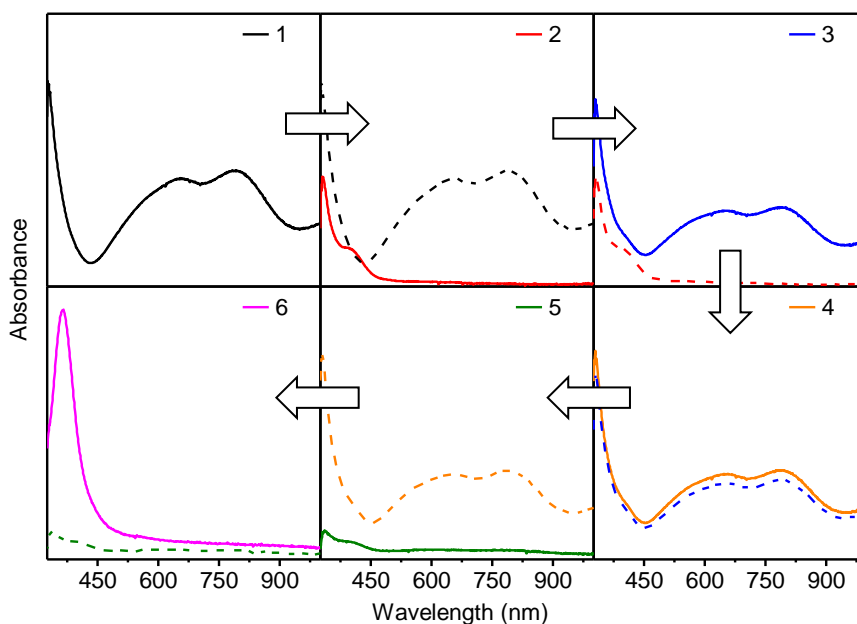
Figure S10. UV-Vis traces for H_2O_2 quantification. The absorbances of the spectra were normalized based on solution volume to account for dilution.

3. X-ray Crystallographic Data

The single crystal X-ray diffraction studies were carried out on a Bruker Kappa Photon II CPAD diffractometer equipped with Cu K_α radiation (λ = 1.54178) for **4a**, a Bruker Kappa Photon II CPAD diffractometer equipped with Mo K_α radiation (λ = 0.71073 Å) for **4b**, and a Nonius Kappa diffractometer equipped with a Bruker APEX-II CCD and Mo K_α radiation (λ = 0.71073 Å) for **4c**. Crystals were mounted on MiTeGen Micromounts with Paratone oil, and data were collected in a nitrogen gas stream at 100 K. The data were integrated using the Bruker SAINT software program and scaled using the SADABS software program. Solution by direct methods (SHELXT) produced a complete phasing model for refinement. All nonhydrogen atoms were refined anisotropically by full-matrix least-squares (SHELXL-2014). All carbon bonded hydrogen atoms were placed using a riding model. Their positions were constrained relative to their parent atom using the appropriate HFIX command in SHELXL-2014. Due to the disorder of the Cu positions in the structure, the hydroxide hydrogen atoms were placed at idealized locations and restrained using DFIX commands to fit to the disorder model of each structure. Their thermals were fixed to that of the parent oxygen atom. Platon SQUEEZE was used to remove the electron density from the lattice due to the disordered solvent contribution. **4a** and **4b** both had 4 voids with 34 electrons in each. **4c** had 2 large voids of 600 electrons. In all cases, the disordered solvent appeared to be a mixture of acetone and diethyl ether.
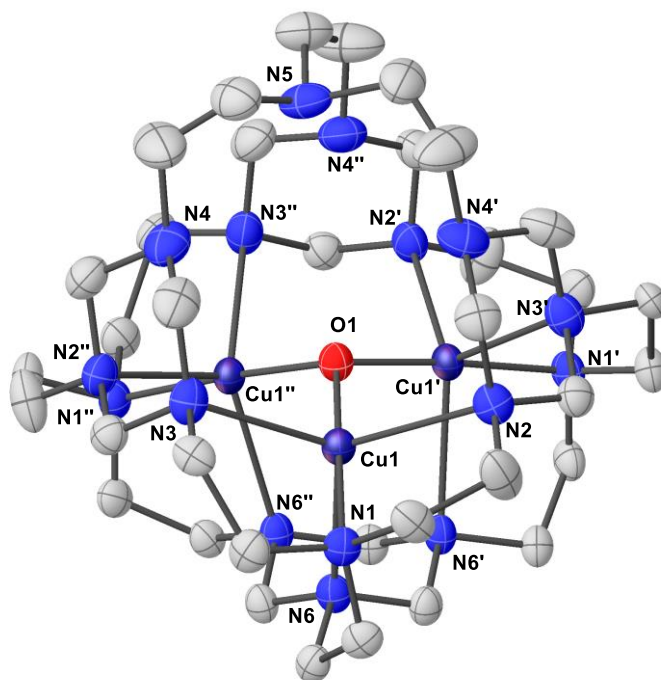
Figure S11: X-ray structure (CIF: 1984893, 100 K) of **4a** with thermal ellipsoids of 20% probability. Hydrogen atoms and anion PF_6^- are omitted for clarity. Selected bond lengths (Å) for **4a**: Ave. Cu–O = 1.885(5), Ave. Cu⋯Cu = 3.098, Cu–N = 2.057-2.538.
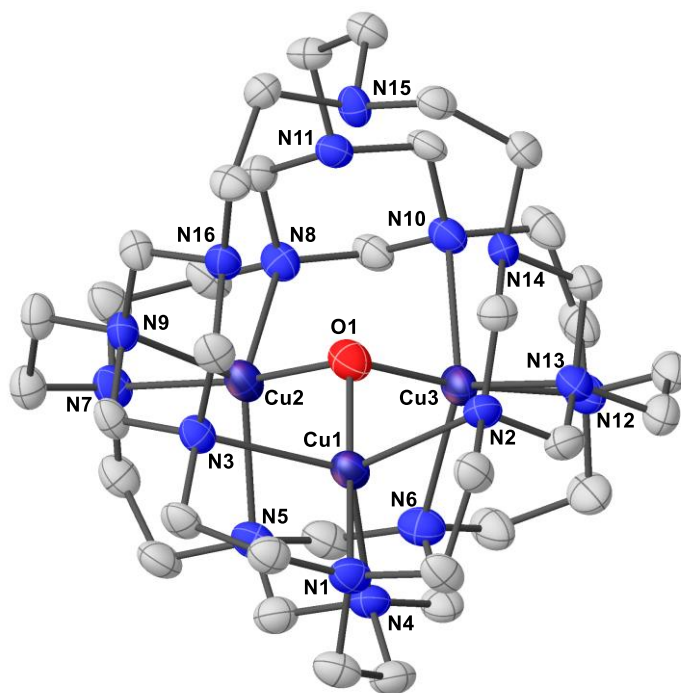
Figure S12: X-ray structure (CIF: 1984894, 100 K) of **4b** with thermal ellipsoids of 50% probability. Hydrogen atoms, solvent molecules, and anion PF_6^- are omitted for clarity. Selected bond lengths (Å) for **4b**: Ave. Cu–O = 1.913(6), Ave. Cu···Cu = 3.112, Cu–N = 2.060-2.491.
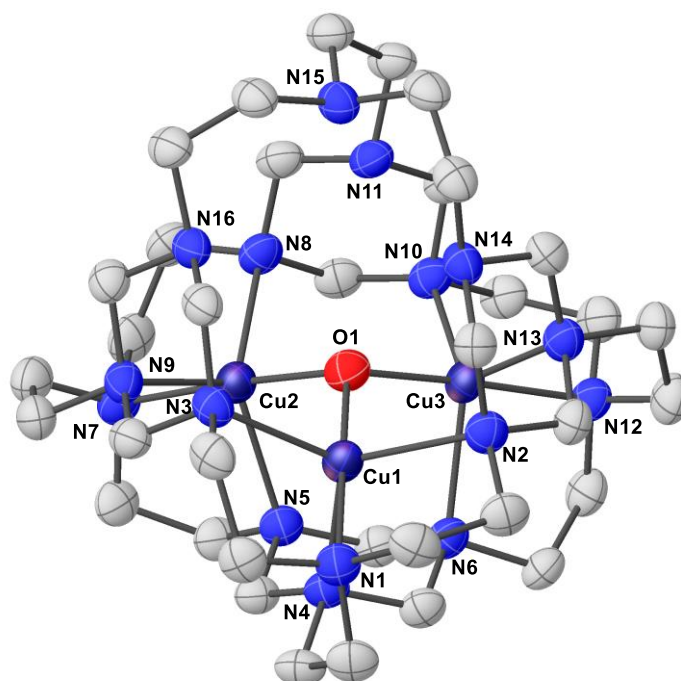
Figure S13: X-ray structure (CIF: 1984895, 100 K) of **4c** with thermal ellipsoids of 30% probability. Hydrogen atoms, solvent molecules, and anion BF_4^-/PF_6^- are omitted for clarity. Selected bond lengths (Å) for **4c**: Ave. Cu–O = 1.937(3), Ave. Cu···Cu = 3.181, Cu–N = 2.093-2.300.
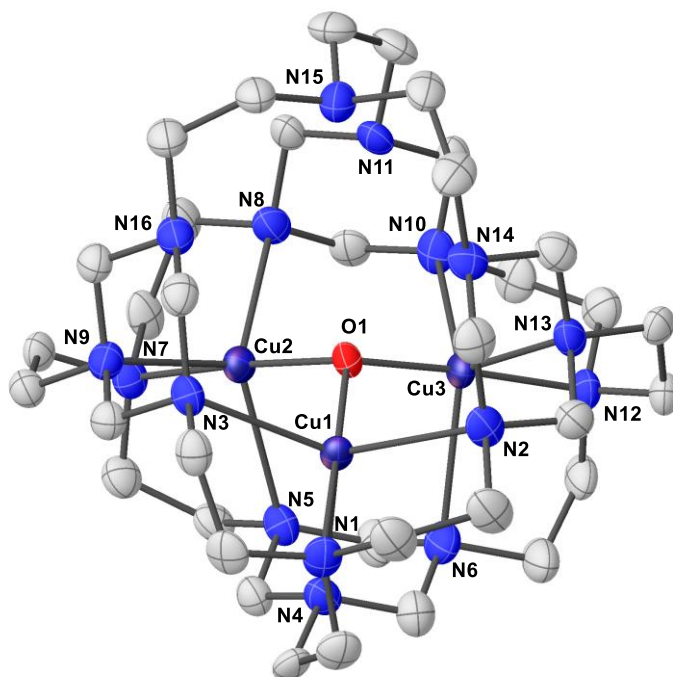
Figure S14: X-ray structure (CIF: 1987932, 100 K) of **4a**-BAr$^F_4$ with thermal ellipsoids of 50% probability. Hydrogen atoms, solvent molecules, and anion BAr$^F_4{}^-$ are omitted for clarity. Selected bond lengths (Å) for **4a**-BAr$^F_4$: Ave. Cu–O = 1.913(2), Ave. Cu···Cu = 3.129, Cu–N = 2.049-2.559.

Table S2: Crystal Data and Structure Refinement for **4a**, **4b**, **4c**, and **4a-**BAr$^F_4$.

	4a	**4b**	**4c**	**4a**-BAr$^F_4$
CCDC	1984893	1984894	1984895	1987932
Empirical formula, FW (g/mol)	$C_{36}H_{73}Cu_3F_{12}N_{16}OP_2$, 1226.64	$C_{45}H_{91}Cu_3F_{18}N_{16}O_4P_3$, 1545.70	$C_{39}H_{79}B_3Cu_3F_{18}N_{16}O_2P$, 1400.20	$C_{100}H_{97}B_2Cu_3F_{48}N_{16}O$, 2663.17
Color	Colorless Block	Blue Block	Blue Block	Colorless Block
Temperature (K)	100	100	100	100
Wavelength (Å)	1.54178	0.71073	0.71073	0.71073
Crystal system, Space group	Cubic, Pa-3	Monoclinic, C 1 c 1	Monoclinic, C 1 2/c 1	Triclinic, P-1
Unit cell dimensions a (Å)	17.4900(2)	22.6031(11)	35.673(3)	12.4878(13)
b (Å)	17.4900(2)	17.2489(8)	21.1666(16)	15.1031(17)
c (Å)	17.4900(2)	17.6361(8)	21.0194(17)	15.1131(17)
α(°)	90°	90	90	77.567(3)
β(°)	90°	100.981(2)	102.442(2)	88.651(3)
γ(°)	90°	90	90	85.637(3)
Volume (Å^3)	5350.19(18)	6750.0(5)	15498(2)	2775.4(5)
Z	4.00008	4	8	1
Density (calc., g/cm^{-3})	1.523	1.521	1.200	1.593
Absorption coefficient (mm^{-1})	2.729	1.108	0.917	0.706
F(000)	2536	3196	5760	1346

Theta range for data collection (°)	6.198 to 68.078	2.932 to 25.393	1.126 to 25.437	3.113 to 25.380
Index ranges	-20<=h<=19, -20<=k<=20, -16<=l<=20	-27<=h<=27, -20<=k<=20, -20<=l<=21	-42<=h<=43, -25<=k<=25, -25<=l<=24	-15<=h<=15, -18<=k<=18, -18<=l<=18
Reflections collected	33351	82474	205973	111075
Independent reflections, R_{int}	1628 [R(int) = 0.0331, R(sigma) = 0.0104]	12117 [R(int) = 0.0465, R(sigma) = 0.0347]	14249 [R(int) = 0.0763, R(sigma) = 0.0452]	10153 [R(int) = 0.0801, R(sigma) = 0.0439]
Completeness to $2\theta_{max}$ (%)	99.4	99.2	99.9	99.8
Absorption correction	Semi-empirical from equivalents	Semi-empirical from equivalents	Semi-empirical from equivalents	Semi-empirical from equivalents
Refinement method	Full-matrix least-squares on F^2	Full-matrix least-squares on F^2	Full-matrix least-squares on F^2	Full-matrix least-squares on F^2
Data / restraints / parameters	1628 / 196 / 201	12117 / 194 / 867	14249 / 52 / 837	10153 / 564 / 1124
Goodness-of-fit	1.047	1.037	1.028	1.128
Final R indices [I>2sigma(I)]	R1 = 0.0679, wR2 = 0.1844	R1 = 0.0530, wR2 = 0.1221	R1 = 0.0616, wR2 = 0.1770	R1 = 0.0791, wR2 = 0.1663
Largest diff. peak and hole ($e \cdot$ Å^{-3})	0.359 and -0.218	0.479 and -0.470	0.732 and -0.316	0.409 and -0.546

4. ESI-MS details

ESI-MS analysis of the reaction of complex 4a and $^{18}O_2$ in the presence of acetic acid

To an acetone solution (5 mL) of complex **4b** (2.2 mg, 0.0016 mmol) in a 20 mL scintillation vial equipped with a septum, CoCp$_2$ (0.27 mg, 0.0015 mmol) was added under nitrogen atmosphere to generate complex **4a** in situ. Excess $^{18}O_2$ (0.5 mL, 0.02 mmol) and acetic acid (2.1 mg, 0.035 mmol) was inject to the vial and the obtained mixture was allowed to stir at room temperature for five minutes, during which the color of the solution changed from yellow to blue, indicating complex **4a** was oxidized back to complex **4b**. ESI-MS analysis of the resulting blue solution (Figure S15) showed that less than 10% of μ_3-^{16}O ligand in **4a** was replaced by ^{18}O during its aerobic oxidation to **4b**.
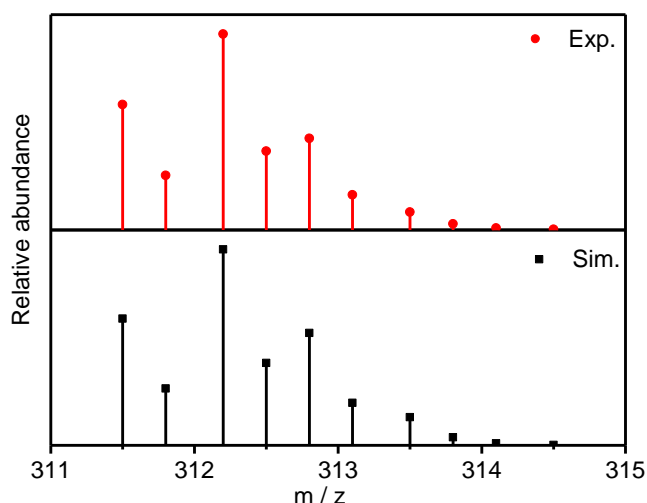
Figure S15. ESI-MS analysis of complex **4b** from the reaction of complex **4a** and $^{18}O_2$ in the presence of acetic acid (red), and simulated mass spectrum with 90% **4b**-^{16}O and 10% **4b**-^{18}O (black).

5. X-band EPR details

EPR spectra were recorded on a Bruker EMXPlus X-band EPR spectrometer equipped with Coldedge cryostat with small-volume power saturation. All samples were measured in 4 mm septum-capped EPR quartz tubes (Wilmad Lab glass, 727-SQ-250MM). Complex **4b** (4.1 mg, 3 μmol) was dissolved in acetonitrile (6.0 mL) to make a 0.50 mM solution of **4b**, and 0.20 mL of the solution was transferred into the EPR tube under nitrogen atmosphere, frozen in liquid nitrogen, and used for EPR measurement. The spectrum was collected at 50 K with a modulation frequency of 100 kHz and a modulation amplitude of 10 G using 30 dB attenuation. A time constant of 40.96 ms and a conversion time of 50.15 ms were used. All spectra were baseline-corrected using Igor Pro (Wavemetrics, Lake Oswego, OR) software. Spectral simulations were performed using the EasySpin toolbox with MATLAB.[2]
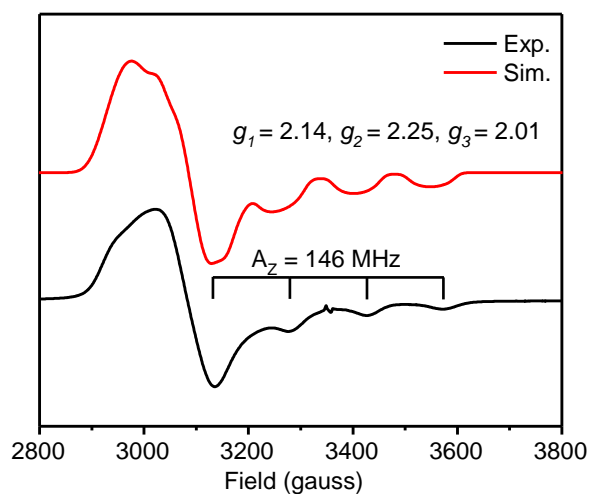
Figure S16. X-band EPR spectrum (frozen MeCN, 50K, 0.5 mM) of complex **4b**; $g_1 = 2.14$, $g_2 = 2.25$, $g_3 = 2.01$, $A_3 = 146$ MHz.

6. Electrochemistry details
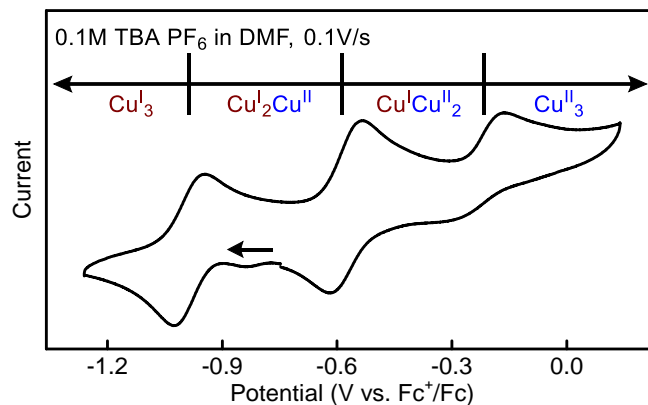
Figure S17. Solution cyclic voltammogram of **4b** (1 mM) in DMF (0.1 M TBAPF$_6$) with a scan rate of 0.100 V/s. Working electrode: glassy carbon; counter electrode: Pt wire; reference electrode: Ag/AgNO$_3$.
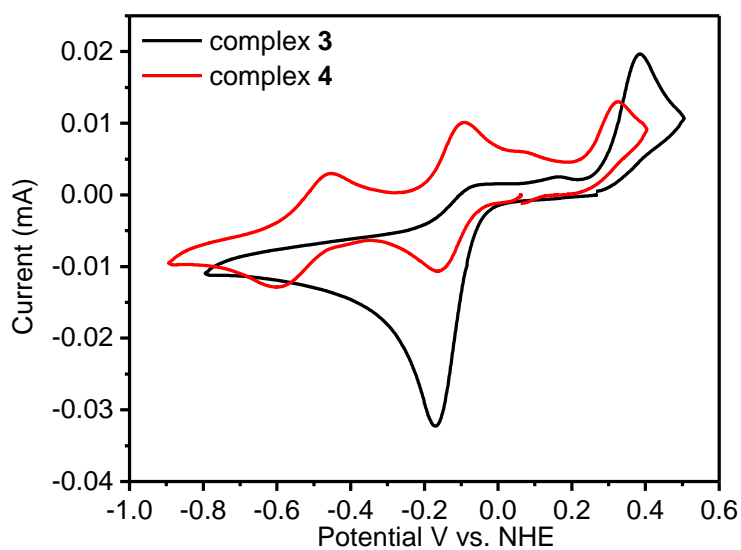
Figure S18. Solution cyclic voltammogram of **4** (1 mM) and **3** (1 mM) in phosphate buffer (pH = 5.8, 0.1 M) with a scan rate of 0.100 V/s. Working electrode: glassy carbon; counter electrode: Pt wire; reference electrode: leakless Ag/AgCl electrode (eDAQ).
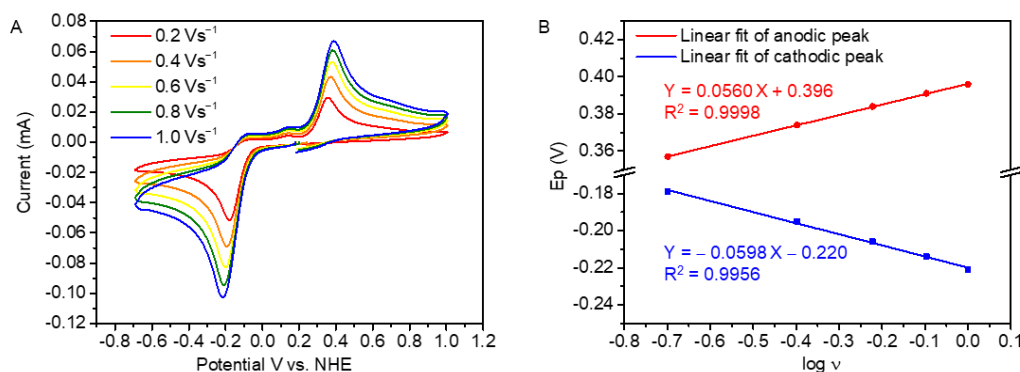
Figure S19. (A) Scan rate dependant cyclic voltammetry of **3a** (1 mM, pH = 5.8 phosphate buffer). (B) Plot of cathodic and anodic potentials against log ν (scan rate, V/s). The number of electrons involved in the redox process can be calculated using Laviron's equation.[3] The slope obtained from the plot is equal to:

$$\frac{2.3RT}{\alpha Fn}$$

where α is the electron-transfer coefficient and assumed to be 0.5 for irreversible process.[4] R ($8.314 \ J \cdot K^{-1} \cdot mol^{-1}$) is the ideal gas constant. T (298K) is temperature. F ($96485 \ C \cdot mol^{-1}$) is Faraday constant. n is the number of electrons involved. n_c, the number of electrons involved in the cathodic process, was calculated to be 2.0. And n_a, the number of electrons involved in the anodic process, was calculated to be 2.1. This result suggests that both the oxidation and the reduction are two-electron processes.
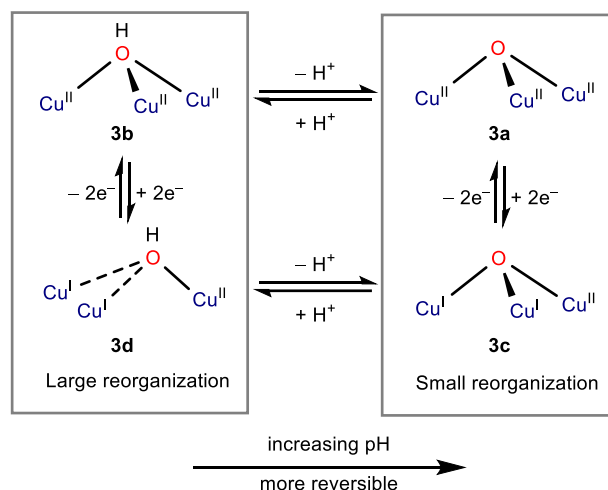
Scheme S2. Proposed redox behavior of **3a** based on its CV at different pH. Under acidic conditions, **3a** is protonated to form **3b** with a μ_3-hydroxo ligand. The *ca.* 800 μV separation of the redox couple at low pH indicates a substantial barrier for electron transfer. Under basic conditions, **3b** is deprotonated to afford **3a**. The central μ_3-oxo ligand in **3a** binds to the three copper centers tighter than μ_3-hydroxo, attenuating the redox-induced geometric change and lowering the barrier for electron transfer. Consequently, the redox of **3a** is more reversible under basic conditions.

Evaluation of the electron self-exchange rate constants k_{el} and k_{hom}.

The standard electrochemical electron self-exchange rate constant k_{el} (cm s^{-1}) for the **4a/4b**

and **4b**/**4c** redox couples was estimated using an electrochemical method published previously.[5] Under quasi-reversible conditions, k_{el} can be derived from Eq. 1:[6,7]

$$\Psi = k_{el}(D_R/D_O)^{\alpha/2}(RT/nF\pi D_R)^{1/2}\nu^{-1/2} \qquad (1)$$

where Ψ is a kinetic parameter, D_R and D_O are the diffusion coefficients (cm^2/s) of the reduced and oxidized species, respectively, α is the transfer coefficient for the electrode process, R is gas constant (8.314 J K^{-1} mol^{-1}), T is temperature (T = 298.15 K in this case), n is the number of electrons transferred in each step (n = 1 in this case), F is Faraday constant (96485.3 C mol^{-1}), and ν is the potential scan rate (V s^{-1}). The kinetic parameter Ψ is also related to the peak-to-peak separation (ΔE_p / mV) of the anodic and cathodic waves in cyclic voltammogram by using the empirical equation (Eq. 2):[6]

$$\Psi = (-0.6288+0.0021n\Delta E_p)/(1-0.017n\Delta E_p) \qquad (2)$$

where n is the number of electrons transferred in each step. Cyclic voltammograms of **4a**/**4b** and **4b**/**4c** (1 mM in MeCN + 0.1 M Bu$_4$NPF$_6$) were measured at different potential scan rates (0.5-5.0 V s^{-1} range) in the suitable potential regions (Figure S20A and S20C). Current interrupt (CI) measurement was performed before the cyclic voltammetry to account for uncompensated resistance (R_u). The values of Ψ were calculated from the experimental ΔE_p values (80 mV – 140 mV) using the Eq. 2. The value of D_O and D_R was obtained using the Randles-Sevcik equations ($9.4(6)\times10^{-7}$ cm^2 s^{-1} and $9.4(6)\times10^{-7}$ cm^2 s^{-1} for **4a**/**4b** redox couple; $1.5(1)\times10^{-6}$ cm^2 s^{-1} and $1.4(1)\times10^{-6}$ cm^2 s^{-1} for **4b**/**4c** redox couple). Since $D_O \approx D_R$ in both redox cases and $0< \alpha <1$, $(D_R/D_O)^{\alpha/2}$ is approximated equal to 1.[7] An estimate of the values of k_{el} was obtained from the Ψ vs $\nu^{-1/2}$ plot using Eq. 1 ($7.8(2)\times10^{-3}$ cm s^{-1} for **4a**/**4b** redox couple, FigureS19B; $7.6(2)\times10^{-3}$ cm s^{-1} for **4b**/**4c** redox couple, FigureS19D). A correlation between k_{el} and the homogeneous electron self-exchange rate constant k_{hom} (L mol^{-1} s^{-1}) has been described by Weaver et al. (Eq. 3):[8]

$$k_{hom} = 4\pi N_A r_h^2 k_{el}10^{-19} \qquad (3)$$

where k_{el} is the electrochemical rate constant (cm s^{-1}), N_A is the Avogadro constant (mol^{-1}), and r_h is the internuclear distance for self-exchange (Å). The value of r_h (11.2 Å) was estimated based on atomic coordinate of the X-ray single-crystal structure **4b** using chemcraft software. The value of k_{hom} was calculated as $7.4(2)\times10^5$ L mol^{-1} s^{-1} for **4a**/**4b** redox couple and $7.2(2)\times10^5$ L mol^{-1} s^{-1} for 4b/4c redox couple.
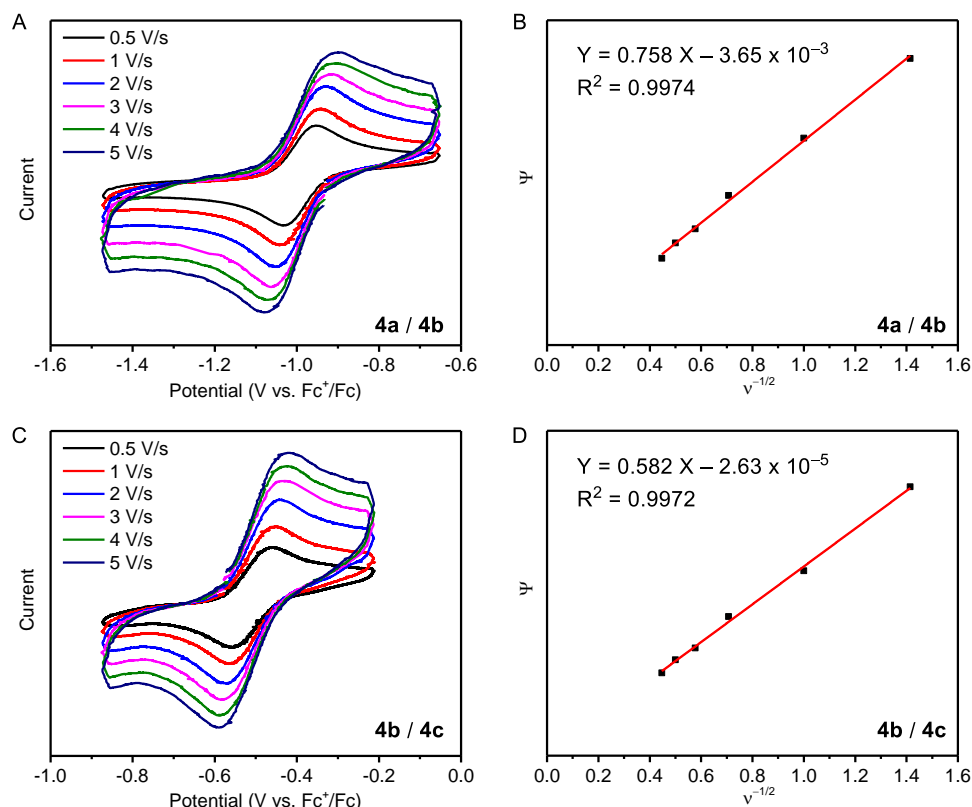
Figure S20. Scan rate dependent cyclic voltammograms for **4a**/**4b** redox couple (A) and **4b**/**4c** redox couple (C). Ψ vs $v^{-1/2}$ plots for **4a**/**4b** redox couple (B) and **4b**/**4c** redox couple (D).

7. Computational details

All computations were performed using ORCA software packages.[9] The geometry optimization was carried out using BP86 method with a mixed basis set (def2-TZVP for the copper atoms and def2-SVP for all light atoms, C, N, O, H), followed by a frequency calculation. For both complex **3** and **4** in $Cu^ICu^{II}Cu^{II}$ and $Cu^{II}Cu^{II}Cu^{II}$ oxidation states, the structures were optimized at three spin states (singlet, triplet, broken symmetry triplet for $Cu^ICu^{II}Cu^{II}$; doublet, quartet, and broken symmetry quartet for $Cu^{II}Cu^{II}Cu^{II}$) at BP86/def2-TZVP(Cu)/def2-TZVP(C, N, O, H) level of theory to determine the ground state (Table S3). To estimate the reorganization energy (λ), single-point calculations of the one-electron oxidized or reduced species at their redox counterpart's geometry were performed. The implication of reorganization energy for the oxidized complex (λ_{ox}) and the reduced complex (λ_{red}) of a redox couple is clarified in Figure S21. The total inner-sphere reorganization energy for a self-exchange reaction (λ_i) is the sum of λ_{ox} and λ_{red}. Solvated single-point energies were calculated at TPSSh/def2-TZVP(Cu)/def2-SVP(C, N, O, H) level[10] with a Solvation Model based on Density (SMD, acetonitrile).[11] Dispersion corrections with Becke-Johnson damping were applied for single-point calculation.[12,13] The Gibbs free energy of each species was determined by adding the solvated single point SCF energy to the thermal correction from the respective frequency calculation.[14] The results are shown in Table S4. Time-dependent density-functional theory (TD-DFT) calculation for complex **4b** and **4c** were performed at BP86/def2-TZVP level using 50 roots.

Oxidation state	Spin state	[TREN$_3$Cu$_3$O]/Ha	[TREN$_4$Cu$_3$OH]/Ha
I II II	Singlet	−6599.04390513[a,b]	–
	Triplet	−6599.04831111[a,b]	Exp. Ground state
	Triplet Broken-symmetry	−6599.04390608[a,b]	–
II II II	Doublet	−6598.55474903[a,b]	−7285.19694591[a,b]
	Quartet	−6598.55615692[a,b]	−7285.19896527[a,b]
	Quartet Broken-symmetry	−6598.55475856[a,b]	−7285.19535823[a,b]

a: BP86/SVP; b: SCF single point energy

Table S3: Ground state determination of complex **3** and **4** at the Cu^{I}Cu^{II}Cu^{II} and Cu^{II}Cu^{II}Cu^{II} oxidation states. The isolated [TREN$_4$Cu$_3$OH] in Cu^{I}Cu^{II}Cu^{II} oxidation has a paramagnetic ^{1}H NMR, which suggests its triplet ground state.
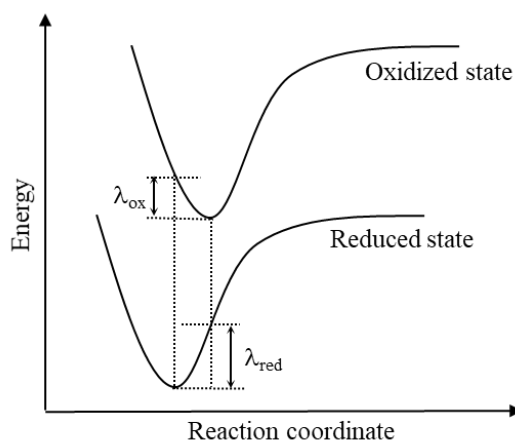
Figure S21. The potential energy of a general electron-transfer process. The reorganization energy of the reduction and the oxidation (λ_{ox} and λ_{red}) are indicated.

Complex	Redox couple	λ_{ox}	λ_{red}	λ_i
Complex **4**	I,I,I − I,I,II	0.047	0.65	0.70
	I,I,II − I,II,II	0.027	0.39	0.42
	I,II,II − II,II,II	0.13	0.046	0.18
Complex **3**	I,I,I − I,I,II	1.1	0.95	2.1
	I,I,II − I,II,II	0.15	0.53	0.68
	I,II,II − II,II,II	0.084	0.26	0.34

Table S4. The calculated λ_{ox}, λ_{red}, and λ_i (eV) for complex **3** and **4**.
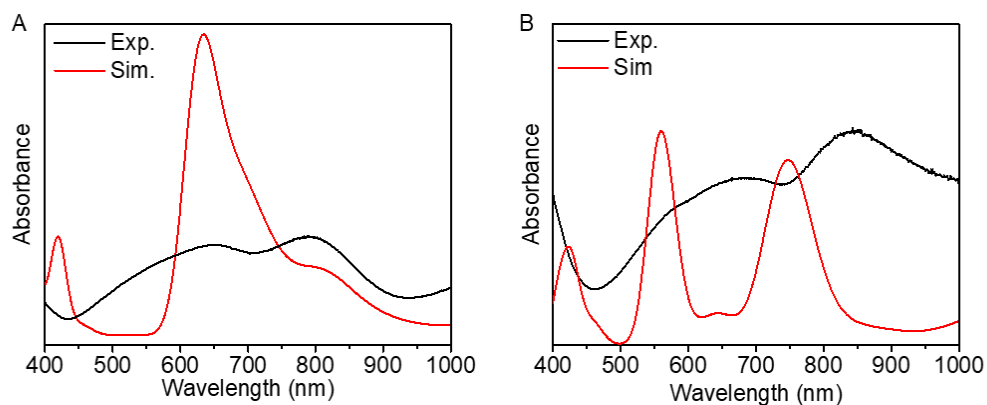
Figure S22. Experimental and simulated UV-vis spectrum of complex **4b** (A) and **4c** (B).

Transitions (nm)	Donor orbital	Acceptor orbital
630 nm		
683 nm		
823 nm		

Table S5: Selected TD-DFT transitions for **4b**. Orbitals plotted at a 0.048 isosurface value.
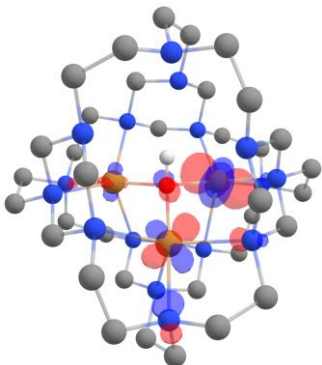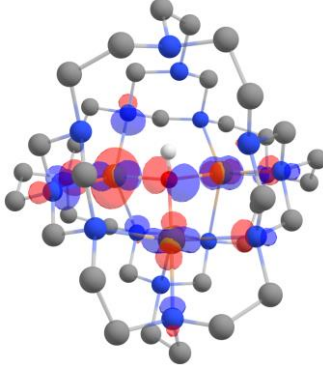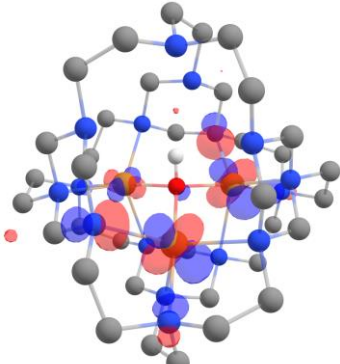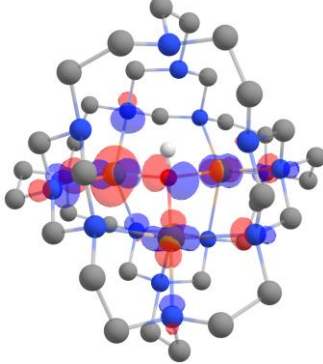
Transitions (nm)	Donor orbital	Acceptor orbital
561 nm		
745 nm		

Table S6: Selected TD-DFT transitions for **4c**. Orbitals plotted at a 0.048 isosurface value.

Cartesian coordinates of complexes used in computations

Complex – Level of theory optimized (Calculations used for)
Charge, spin multiplicity

[TREN₄Cu^ICu^ICu^I(u_3-OH)] – BP86/def2-SVP (C, H, O, N)/def2-TZVP (Cu)
2, 1

29	9.733391000	-0.179256000	10.360415000
6	10.982866000	2.011531000	12.156563000
1	11.025418000	2.878547000	12.864461000
1	12.009104000	1.913309000	11.746150000
6	8.394227000	-1.447503000	12.936769000
1	7.985615000	-2.246915000	13.606288000
1	8.085973000	-0.488172000	13.402451000
7	7.805923000	-1.495428000	11.593444000
6	9.919155000	-1.572553000	12.945956000
1	10.265463000	-1.593725000	14.006910000
1	10.208664000	-2.549079000	12.510799000
7	10.642610000	-0.508729000	12.190831000
7	11.791656000	-1.584373000	9.582177000
7	12.160309000	-0.182954000	7.675744000
7	11.009843000	-2.284982000	7.415317000
6	10.621100000	0.765416000	12.970879000
1	11.315256000	0.693894000	13.841371000
1	9.607250000	0.884495000	13.400234000

S22

6	11.554433000	-2.725960000	8.702771000
1	10.826684000	-3.402991000	9.196248000
1	12.509034000	-3.313851000	8.540103000
6	7.797845000	-2.849105000	11.039747000
1	7.209797000	-3.545175000	11.712482000
1	8.837605000	-3.232061000	10.990502000
6	12.060197000	-0.937458000	11.985616000
1	12.484165000	-1.318461000	12.944471000
1	12.653522000	-0.038392000	11.728707000
6	11.916571000	-1.311899000	6.791432000
1	11.444677000	-0.951305000	5.856688000
1	12.892217000	-1.815181000	6.504521000
6	12.715981000	-0.648758000	8.934966000
1	12.873972000	0.226339000	9.596813000
1	13.725895000	-1.145574000	8.790588000
6	12.365345000	1.643691000	5.927806000
1	12.066134000	0.948454000	5.119042000
1	13.170375000	2.282705000	5.475675000
6	12.254622000	-2.006231000	10.906266000
1	13.334921000	-2.299115000	10.907353000
1	11.699070000	-2.927608000	11.179993000
6	13.013790000	0.840734000	7.063088000
1	13.325627000	1.529292000	7.875897000
1	13.965855000	0.403484000	6.662554000
29	8.570128000	-1.616729000	7.759195000
6	10.759997000	-3.415140000	6.512144000
1	11.626383000	-4.123852000	6.470437000
1	10.663181000	-3.004541000	5.485846000
6	7.297324000	-4.191754000	9.096962000
1	6.496666000	-4.860431000	9.504539000
1	8.255761000	-4.658520000	9.406361000
7	7.250146000	-2.848421000	9.685257000
6	7.173981000	-4.200765000	7.571885000
1	7.152001000	-5.261691000	7.225534000
1	6.198205000	-3.764556000	7.281421000
7	8.239397000	-3.446797000	6.849592000
7	7.167663000	-0.837004000	5.699587000
7	8.571409000	1.068012000	5.332419000
7	6.468452000	1.330575000	6.480667000
6	9.512660000	-4.228235000	6.872456000
1	9.440986000	-5.098560000	6.178108000
1	9.630089000	-4.657821000	7.886400000
6	6.026716000	0.043544000	5.935708000
1	5.348495000	-0.449201000	6.662854000
1	5.439820000	0.206719000	4.980574000
6	5.897063000	-2.293234000	9.691639000
1	5.199485000	-2.965411000	10.278559000
1	5.515566000	-2.243293000	8.651368000
6	7.812398000	-3.241093000	5.431568000
1	7.430813000	-4.199527000	5.007176000
1	8.712370000	-2.985166000	4.839186000
6	7.443065000	1.953449000	5.574906000
1	7.804023000	2.887907000	6.047085000
1	6.941071000	2.240711000	4.598702000
6	8.104871000	-0.190704000	4.776215000

1	8.979431000	-0.853455000	4.619068000
1	7.609227000	-0.045760000	3.765810000
6	10.400064000	2.814039000	5.129437000
1	9.705361000	3.623515000	5.427949000
1	11.040438000	3.265569000	4.325145000
6	6.744938000	-2.160632000	5.236071000
1	6.453228000	-2.161334000	4.155458000
1	5.822680000	-2.433456000	5.790602000
6	9.596610000	1.679672000	4.480024000
1	10.284614000	0.866169000	4.168776000
1	9.160726000	2.080752000	3.527569000
29	7.133732000	0.985916000	8.921374000
8	8.864795000	0.114946000	8.628418000
6	5.338977000	2.234920000	6.729351000
1	4.631238000	2.277421000	5.862207000
1	5.750538000	3.260785000	6.826652000
6	4.555728000	-0.349247000	10.191094000
1	3.885707000	-0.756137000	10.990979000
1	4.089734000	-0.658122000	9.232121000
7	5.898404000	-0.938916000	10.239760000
6	4.548128000	1.175837000	10.314442000
1	3.487539000	1.523286000	10.335069000
1	4.983412000	1.465885000	11.290749000
7	5.304154000	1.897357000	9.249956000
7	7.914007000	3.044624000	10.324605000
7	9.820901000	3.409892000	8.922948000
7	10.080044000	2.261255000	11.026109000
6	4.524155000	1.875382000	7.975786000
1	3.654443000	2.570607000	8.046523000
1	4.093660000	0.861886000	7.857809000
6	8.793068000	2.807526000	11.466465000
1	8.298766000	2.080822000	12.144011000
1	8.956602000	3.762412000	12.053660000
6	6.452076000	-0.946087000	11.593432000
1	5.778675000	-1.532507000	12.290236000
1	6.502607000	0.094087000	11.975118000
7	11.190965000	2.436277000	6.304654000
6	5.510863000	3.315137000	9.677308000
1	4.552460000	3.740484000	10.057906000
1	5.768349000	3.907361000	8.777676000
6	10.704860000	3.166496000	10.052221000
1	11.639265000	2.693447000	9.692246000
1	10.992563000	4.142349000	10.554636000
6	8.562235000	3.967362000	9.388103000
1	7.900606000	4.125176000	8.512814000
1	8.707665000	4.977604000	9.883931000
6	11.569065000	3.611045000	7.096077000
1	12.377493000	3.311640000	7.791626000
1	12.022140000	4.414918000	6.456272000
6	6.590379000	3.509413000	10.745946000
1	6.590425000	4.589988000	11.037810000
1	6.316022000	2.954997000	11.667822000
6	10.434482000	4.261588000	7.898321000
1	9.622012000	4.573522000	7.209407000
1	10.836021000	5.213710000	8.334511000

1	9.434252000	0.683367000	8.059623000

[TREN₄Cu^ICu^ICu^II(μ₃-OH)] – BP86/def2-SVP (C, H, O, N)/def2-TZVP (Cu)

3, 2

29	9.867699000	-0.252278000	10.297176000
6	11.003535000	1.970426000	12.057747000
1	11.027273000	2.896362000	12.683653000
1	12.024885000	1.869689000	11.635057000
6	8.397633000	-1.340594000	12.894941000
1	7.894433000	-2.111376000	13.528052000
1	8.098392000	-0.362154000	13.324360000
7	7.909043000	-1.372691000	11.499656000
6	9.907769000	-1.530610000	13.016478000
1	10.185168000	-1.512097000	14.095906000
1	10.190401000	-2.537853000	12.651056000
7	10.696260000	-0.522880000	12.255915000
7	11.658692000	-1.548835000	9.652030000
7	12.068763000	-0.138308000	7.751116000
7	10.860800000	-2.234046000	7.451121000
6	10.699457000	0.785005000	12.971991000
1	11.440417000	0.775505000	13.804403000
1	9.713253000	0.918153000	13.456622000
6	11.408508000	-2.684620000	8.746904000
1	10.690042000	-3.373686000	9.232315000
1	12.365953000	-3.249867000	8.576365000
6	7.897300000	-2.740753000	10.972296000
1	7.256819000	-3.402649000	11.623795000
1	8.924484000	-3.155875000	10.987740000
6	12.091369000	-1.009883000	12.057090000
1	12.498026000	-1.443772000	12.999191000
1	12.732425000	-0.137420000	11.822924000
6	11.785443000	-1.238275000	6.845599000
1	11.309599000	-0.844782000	5.928537000
1	12.734381000	-1.767282000	6.538872000
6	12.629431000	-0.645323000	8.988749000
1	12.860459000	0.205856000	9.658056000
1	13.593307000	-1.210179000	8.821449000
6	12.375517000	1.654369000	5.969708000
1	12.108602000	0.953654000	5.154203000
1	13.204196000	2.280823000	5.548643000
6	12.195466000	-2.049727000	10.942542000
1	13.257632000	-2.374651000	10.846843000
1	11.622521000	-2.960662000	11.213506000
6	12.966919000	0.863844000	7.142286000
1	13.263991000	1.560859000	7.952600000
1	13.918938000	0.393563000	6.787675000
29	8.693098000	-1.653489000	7.762670000
6	10.734697000	-3.376168000	6.505207000
1	11.657575000	-4.003152000	6.497111000
1	10.654784000	-2.945198000	5.486202000
6	7.408799000	-4.161876000	9.099819000
1	6.620123000	-4.776445000	9.597903000
1	8.376452000	-4.613473000	9.402750000
7	7.404152000	-2.765305000	9.589209000
6	7.221567000	-4.269832000	7.589235000

1	7.220524000	-5.346285000	7.300868000
1	6.224394000	-3.880469000	7.306773000
7	8.245960000	-3.517862000	6.815302000
7	7.207595000	-0.861474000	5.842430000
7	8.616212000	1.027267000	5.412652000
7	6.542923000	1.340993000	6.650146000
6	9.532085000	-4.272614000	6.791161000
1	9.500306000	-5.087777000	6.031746000
1	9.656925000	-4.779218000	7.767849000
6	6.083012000	0.035820000	6.120847000
1	5.422322000	-0.448092000	6.867709000
1	5.474328000	0.209777000	5.187999000
6	6.044128000	-2.207727000	9.560324000
1	5.347658000	-2.870012000	10.152354000
1	5.672842000	-2.187900000	8.516808000
6	7.757923000	-3.271289000	5.427238000
1	7.327802000	-4.204184000	4.995779000
1	8.632342000	-3.020866000	4.794885000
6	7.521173000	1.935401000	5.701109000
1	7.919352000	2.861565000	6.155790000
1	6.975306000	2.227476000	4.755882000
6	8.095749000	-0.211396000	4.863525000
1	8.943494000	-0.884700000	4.628726000
1	7.530443000	-0.040758000	3.897952000
6	10.414946000	2.787609000	5.096288000
1	9.725676000	3.616420000	5.351278000
1	11.060921000	3.194888000	4.275908000
6	6.713569000	-2.157303000	5.337840000
1	6.366249000	-2.087150000	4.278590000
1	5.812764000	-2.430868000	5.926270000
6	9.610004000	1.626828000	4.503998000
1	10.296094000	0.810506000	4.196426000
1	9.135869000	1.989436000	3.556522000
29	7.153099000	1.134582000	8.851469000
8	8.852851000	0.142821000	8.617909000
6	5.395216000	2.279248000	6.765410000
1	4.781077000	2.285551000	5.833364000
1	5.815684000	3.301998000	6.856736000
6	4.616964000	-0.351698000	10.058400000
1	3.987080000	-0.862990000	10.827099000
1	4.186235000	-0.645259000	9.078350000
7	6.013546000	-0.838008000	10.086433000
6	4.486469000	1.155570000	10.260945000
1	3.405054000	1.424722000	10.263047000
1	4.868105000	1.433780000	11.262714000
7	5.222904000	1.957218000	9.246379000
7	7.858852000	2.892031000	10.236735000
7	9.761280000	3.354026000	8.853719000
7	10.073115000	2.108180000	10.914385000
6	4.483128000	1.977992000	7.952198000
1	3.658961000	2.727357000	7.978183000
1	3.989868000	0.996219000	7.817485000
6	8.762336000	2.598128000	11.367512000
1	8.280965000	1.827063000	12.001725000
1	8.891879000	3.526435000	11.993690000

6	6.544982000	-0.831439000	11.454951000
1	5.868848000	-1.424741000	12.137154000
1	6.569121000	0.208091000	11.837911000
7	11.189520000	2.451746000	6.295688000
6	5.445366000	3.344641000	9.746261000
1	4.514042000	3.754980000	10.199241000
1	5.673587000	3.992072000	8.876993000
6	10.665487000	3.064931000	9.954255000
1	11.595177000	2.616441000	9.556937000
1	10.953696000	4.013902000	10.497746000
6	8.521133000	3.894837000	9.369944000
1	7.853624000	4.152111000	8.523929000
1	8.682614000	4.840931000	9.967295000
6	11.532594000	3.651025000	7.067082000
1	12.352925000	3.392721000	7.765211000
1	11.952146000	4.464528000	6.420426000
6	6.578374000	3.420591000	10.767405000
1	6.683214000	4.474788000	11.115915000
1	6.317423000	2.830500000	11.670706000
6	10.368209000	4.256558000	7.859115000
1	9.558553000	4.562678000	7.164755000
1	10.732632000	5.204324000	8.330877000
1	9.437600000	0.695093000	8.040209000

[TREN₄CuᴵCuᴵᴵCuᴵᴵ(μ_3-OH)] – BP86/def2-SVP (C, H, O, N)/def2-TZVP (Cu)

4, 3

29	11.332640000	5.553828000	4.694543000
29	8.952332000	7.914458000	4.637590000
29	10.782927000	7.404710000	7.407496000
8	10.728126000	7.341804000	5.391253000
7	9.616170000	4.313948000	5.914762000
7	7.004834000	8.315041000	3.891774000
7	13.394214000	5.563578000	5.638601000
7	9.573611000	7.906073000	2.464139000
7	8.574436000	9.821341000	5.864378000
7	13.886588000	7.900561000	6.183297000
7	10.804451000	10.644345000	5.480747000
7	11.830757000	3.593115000	4.060469000
7	8.833007000	5.877654000	7.609103000
7	12.839213000	6.498805000	7.837149000
7	12.019460000	8.043439000	2.452275000
7	10.265118000	9.597520000	7.628435000
7	7.817044000	5.871880000	5.392870000
7	10.594959000	7.343738000	9.526794000
7	13.504869000	10.147592000	4.106372000
7	10.957021000	5.878678000	2.436908000
6	8.835050000	9.819209000	7.318437000
6	14.290863000	6.735941000	5.412774000
6	13.288827000	5.305476000	7.092956000
6	13.835220000	7.575184000	7.596097000
6	9.698170000	6.508902000	1.987735000
6	10.777854000	8.682734000	2.046360000
6	6.012640000	7.400587000	4.528065000
6	8.359487000	4.518423000	5.173840000
6	12.083854000	6.696276000	1.917933000

6	7.590734000	6.059726000	6.837337000
6	9.355609000	4.526975000	7.350487000
6	8.503107000	6.040485000	9.051917000
6	12.071523000	3.643784000	2.587335000
6	13.201521000	8.815396000	1.994154000
6	11.093595000	10.607811000	6.905784000
6	9.394515000	10.906608000	5.265402000
6	9.728237000	6.202649000	9.940708000
6	14.804505000	9.641065000	4.556455000
6	11.029381000	4.498088000	1.873197000
6	7.122886000	10.090878000	5.640837000
6	14.025511000	4.384434000	4.962994000
6	10.096522000	2.914800000	5.741302000
6	8.387213000	8.559616000	1.824149000
6	6.687721000	9.736890000	4.222843000
6	10.713885000	2.654776000	4.373085000
6	13.070987000	3.208299000	4.797203000
6	14.803893000	9.045918000	5.967806000
6	9.999058000	8.646347000	9.949359000
6	13.380647000	10.186747000	2.646942000
6	10.500611000	9.801858000	9.093397000
6	12.783744000	6.163184000	9.291537000
6	11.616003000	11.672958000	4.787665000
6	11.972247000	7.182603000	10.082720000
6	6.526706000	5.971951000	4.652861000
6	13.124556000	11.409593000	4.747042000
6	7.058303000	8.104733000	2.414860000
1	8.506616000	10.800415000	7.754380000
1	8.227064000	9.023886000	7.791557000
1	15.343677000	6.426068000	5.667487000
1	14.261605000	6.980916000	4.334870000
1	12.574482000	4.479076000	7.271503000
1	14.287880000	4.979723000	7.486616000
1	14.833021000	7.235759000	7.996032000
1	13.551352000	8.481469000	8.166584000
1	8.845310000	5.914583000	2.369506000
1	9.653207000	6.489019000	0.865855000
1	10.738570000	8.818177000	0.928580000
1	10.712752000	9.685019000	2.508925000
1	5.757955000	7.807589000	5.525189000
1	5.060454000	7.395728000	3.951232000
1	8.543089000	4.379793000	4.091310000
1	7.602564000	3.747940000	5.488227000
1	12.046079000	6.681882000	0.791766000
1	13.044404000	6.234675000	2.219560000
1	6.804504000	5.339345000	7.197215000
1	7.209872000	7.082919000	7.021368000
1	8.626844000	3.755145000	7.725237000
1	10.303066000	4.384040000	7.903980000
1	7.845622000	6.929030000	9.138998000
1	7.898442000	5.182251000	9.430852000
1	13.086094000	4.051268000	2.413061000
1	12.074660000	2.619338000	2.151296000
1	14.092417000	8.184021000	2.193298000
1	13.181917000	8.963118000	0.885876000

1	12.156686000	10.343830000	7.060260000
1	10.917405000	11.613405000	7.383054000
1	9.198961000	10.962388000	4.177053000
1	9.067996000	11.889146000	5.711576000
1	10.339780000	5.280190000	9.929871000
1	9.395455000	6.329360000	10.995940000
1	15.161185000	8.883082000	3.830312000
1	15.591271000	10.436886000	4.542670000
1	10.022605000	4.040016000	1.959712000
1	11.258420000	4.519021000	0.783092000
1	6.552078000	9.494770000	6.381694000
1	6.872501000	11.156352000	5.847511000
1	14.388944000	4.730429000	3.974436000
1	14.930444000	4.044831000	5.516919000
1	10.841042000	2.722993000	6.541054000
1	9.275600000	2.178762000	5.910135000
1	8.511683000	9.653926000	1.956454000
1	8.379043000	8.382026000	0.723993000
1	7.195414000	10.389454000	3.486818000
1	5.598554000	9.934933000	4.107727000
1	9.947300000	2.745598000	3.578558000
1	11.066117000	1.599279000	4.329151000
1	12.777550000	2.805487000	5.786229000
1	13.598017000	2.377566000	4.276849000
1	14.518914000	9.825346000	6.704656000
1	15.858601000	8.770031000	6.218640000
1	8.896704000	8.565593000	9.886837000
1	10.226546000	8.853989000	11.018822000
1	12.528515000	10.843787000	2.380281000
1	14.268442000	10.667286000	2.162961000
1	11.592815000	9.936321000	9.229864000
1	10.029899000	10.748472000	9.445195000
1	12.339611000	5.151680000	9.388175000
1	13.805940000	6.088720000	9.727725000
1	11.217674000	11.752276000	3.754436000
1	11.461469000	12.683710000	5.241020000
1	12.470747000	8.170875000	10.066564000
1	11.931136000	6.876909000	11.151928000
1	6.685430000	5.532871000	3.646291000
1	5.735261000	5.347644000	5.130849000
1	13.537194000	11.423297000	5.775666000
1	13.593460000	12.292298000	4.244279000
1	6.888812000	7.030500000	2.206111000
1	6.227002000	8.643700000	1.907658000
1	11.389142000	8.004095000	5.055192000

[**TREN**₄Cu^{II}Cu^{II}Cu^{II}(μ_3-OH)] – BP86/def2-SVP (C, H, O, N)/def2-TZVP (Cu)

5, 4

29	11.301151000	5.508161000	4.709651000
29	8.903489000	7.865459000	4.645166000
29	10.722745000	7.370986000	7.437181000
8	10.694486000	7.306051000	5.410588000
7	9.618399000	4.319254000	5.887529000
7	6.996634000	8.310187000	3.889444000
7	13.377816000	5.553089000	5.634479000

7	9.552486000	7.893690000	2.467821000
7	8.593633000	9.796404000	5.842628000
7	13.862294000	7.908986000	6.131074000
7	10.854487000	10.602551000	5.492701000
7	11.830244000	3.585372000	4.063099000
7	8.859758000	5.878794000	7.614952000
7	12.814083000	6.523291000	7.822579000
7	12.000379000	8.079358000	2.489587000
7	10.255405000	9.578153000	7.643132000
7	7.812549000	5.898759000	5.399239000
7	10.589229000	7.339924000	9.535021000
7	13.620621000	10.258882000	4.061893000
7	10.970441000	5.882876000	2.466246000
6	8.832210000	9.810266000	7.303379000
6	14.276423000	6.720493000	5.392861000
6	13.272453000	5.319934000	7.094449000
6	13.794148000	7.611253000	7.556015000
6	9.707930000	6.497074000	1.996057000
6	10.747170000	8.685337000	2.051032000
6	5.993844000	7.419421000	4.552346000
6	8.351822000	4.541503000	5.160791000
6	12.096001000	6.720507000	1.970371000
6	7.607095000	6.073630000	6.852980000
6	9.371399000	4.523443000	7.331839000
6	8.521326000	6.007407000	9.069474000
6	12.098997000	3.650799000	2.591252000
6	13.168953000	8.855754000	1.997821000
6	11.097638000	10.584347000	6.931801000
6	9.442770000	10.856371000	5.234452000
6	9.745860000	6.177306000	9.953586000
6	14.861752000	9.636736000	4.520959000
6	11.065947000	4.507318000	1.873209000
6	7.144991000	10.111131000	5.607377000
6	14.019940000	4.359063000	4.982068000
6	10.072126000	2.901686000	5.710231000
6	8.357212000	8.523320000	1.806312000
6	6.706545000	9.747078000	4.195734000
6	10.701046000	2.646225000	4.348936000
6	13.059690000	3.190254000	4.819488000
6	14.820357000	9.026721000	5.927756000
6	9.967253000	8.633301000	9.962204000
6	13.369843000	10.240853000	2.621560000
6	10.463476000	9.796155000	9.117080000
6	12.797496000	6.202098000	9.288918000
6	11.654795000	11.665491000	4.830718000
6	11.977964000	7.210170000	10.081040000
6	6.495219000	5.989398000	4.686737000
6	13.171351000	11.444951000	4.789617000
6	7.037636000	8.069668000	2.413013000
1	8.508926000	10.800196000	7.718658000
1	8.205312000	9.031985000	7.778967000
1	15.324063000	6.418063000	5.670081000
1	14.267870000	6.935830000	4.307913000
1	12.566117000	4.490464000	7.287448000
1	14.272463000	5.008625000	7.493584000

1	14.792968000	7.297930000	7.969270000
1	13.491015000	8.525300000	8.103278000
1	8.856022000	5.888043000	2.355199000
1	9.687398000	6.477461000	0.874920000
1	10.722124000	8.795172000	0.931401000
1	10.650298000	9.699159000	2.483289000
1	5.751346000	7.845699000	5.544398000
1	5.038547000	7.422826000	3.980881000
1	8.519672000	4.409830000	4.075362000
1	7.595161000	3.776211000	5.479077000
1	12.085309000	6.698181000	0.845552000
1	13.055827000	6.275007000	2.295823000
1	6.829393000	5.348723000	7.214110000
1	7.224807000	7.093123000	7.051299000
1	8.637174000	3.757307000	7.699446000
1	10.319427000	4.361321000	7.878288000
1	7.846732000	6.881055000	9.169936000
1	7.933085000	5.130380000	9.426988000
1	13.117751000	4.055839000	2.436761000
1	12.108880000	2.627988000	2.151809000
1	14.070634000	8.232444000	2.166606000
1	13.119539000	9.006193000	0.891484000
1	12.158634000	10.339851000	7.127607000
1	10.893751000	11.593098000	7.386678000
1	9.273697000	10.880769000	4.140515000
1	9.113031000	11.852484000	5.641268000
1	10.373369000	5.265448000	9.939820000
1	9.420168000	6.300017000	11.011338000
1	15.181275000	8.887131000	3.771731000
1	15.680225000	10.400246000	4.529983000
1	10.060435000	4.042998000	1.929688000
1	11.315294000	4.555066000	0.789218000
1	6.553782000	9.549425000	6.358418000
1	6.932536000	11.187571000	5.795587000
1	14.401587000	4.690220000	3.995369000
1	14.913651000	4.024261000	5.555624000
1	10.800654000	2.689537000	6.519089000
1	9.231874000	2.186190000	5.863830000
1	8.472834000	9.621884000	1.905980000
1	8.350827000	8.315235000	0.712243000
1	7.223312000	10.377372000	3.447123000
1	5.620611000	9.958379000	4.074671000
1	9.948116000	2.741403000	3.542121000
1	11.055734000	1.591824000	4.301400000
1	12.752499000	2.792506000	5.806355000
1	13.579453000	2.351309000	4.305175000
1	14.569007000	9.809911000	6.671527000
1	15.865850000	8.715084000	6.172608000
1	8.866719000	8.535853000	9.894758000
1	10.187271000	8.832129000	11.034864000
1	12.509626000	10.903013000	2.404534000
1	14.234751000	10.709961000	2.087121000
1	11.550175000	9.951083000	9.270589000
1	9.970050000	10.735305000	9.455059000
1	12.385645000	5.179515000	9.407572000

1	13.830363000	6.158489000	9.702668000
1	11.260870000	11.777634000	3.799891000
1	11.488434000	12.659937000	5.313237000
1	12.455598000	8.208480000	10.060456000
1	11.945307000	6.909351000	11.151773000
1	6.623884000	5.526484000	3.687065000
1	5.717458000	5.378624000	5.200412000
1	13.599856000	11.417236000	5.809515000
1	13.612769000	12.359634000	4.319886000
1	6.868105000	6.991516000	2.226900000
1	6.196751000	8.596785000	1.909255000
1	11.353151000	7.971043000	5.077297000

[TREN$_3$Cu^{I}Cu^{I}Cu^I(μ_3-O)] – BP86/def2-SVP (C, H, O, N)/def2-TZVP (Cu)

1, 1

29	5.142650000	1.378498000	-2.485868000
7	3.599546000	0.008147000	-3.843059000
6	3.990698000	-1.387176000	-4.160881000
1	3.978414000	-1.951726000	-3.207063000
1	3.219284000	-1.865609000	-4.818215000
6	5.376240000	-1.559008000	-4.822788000
7	6.541422000	-1.138282000	-4.048112000
7	4.964341000	2.630356000	-4.157060000
6	6.092672000	2.376960000	-5.090235000
7	7.353769000	2.666930000	-4.438305000
29	7.828423000	1.225693000	-2.215122000
29	6.425283000	2.750381000	-0.553633000
7	8.102229000	2.913058000	1.158071000
6	9.397202000	2.523003000	0.606058000
7	9.590117000	3.168400000	-0.690685000
7	8.019221000	-1.650082000	-2.143339000
6	6.992811000	-2.122506000	-3.028362000
1	7.365468000	-3.018277000	-3.577727000
6	9.378642000	-1.464161000	-2.607531000
1	10.038602000	-1.381079000	-1.717510000
1	9.702238000	-2.399838000	-3.117526000
6	9.704348000	-0.330805000	-3.615446000
7	9.615471000	1.088967000	-3.108933000
7	3.431167000	0.968776000	-0.963684000
6	2.670818000	-0.161950000	-1.502907000
6	2.382393000	0.024713000	-2.999854000
6	3.436626000	0.839124000	-5.048152000
6	3.657952000	2.337684000	-4.792640000
6	5.024547000	4.052453000	-3.727967000
7	6.306979000	4.333104000	-3.109331000
7	6.019713000	4.703153000	0.000640000
6	7.288307000	5.213551000	0.610700000
6	7.928909000	4.281807000	1.653748000
1	7.307731000	4.248954000	2.572124000
1	8.898871000	4.742375000	1.953238000
1	8.018073000	5.352614000	-0.209391000
1	7.102698000	6.210630000	1.079788000
6	5.589128000	5.639778000	-1.082133000
1	4.530763000	5.421776000	-1.315712000
1	5.614007000	6.687429000	-0.698321000

6	6.398842000	5.597468000	-2.387776000
6	7.409534000	4.064221000	-4.018247000
6	8.523139000	2.167299000	-5.156171000
6	9.763411000	2.022637000	-4.266181000
6	10.720835000	1.335230000	-2.118604000
1	11.701259000	1.177405000	-2.631137000
1	10.636943000	0.550397000	-1.342453000
6	10.757520000	2.732853000	-1.449388000
1	10.989795000	3.508161000	-2.211220000
1	11.640614000	2.728210000	-0.773416000
1	10.042187000	3.016056000	-3.865870000
1	10.618544000	1.697192000	-4.904163000
1	8.245291000	1.181218000	-5.580434000
1	8.810377000	2.814214000	-6.024716000
1	7.387733000	4.748832000	-4.921638000
1	8.361956000	4.255848000	-3.484554000
1	7.473168000	5.781890000	-2.181307000
1	6.057572000	6.471722000	-3.002010000
6	4.948621000	4.583566000	1.049449000
6	3.520463000	4.291071000	0.527384000
7	3.443022000	3.315145000	-0.551065000
6	2.673733000	2.083071000	-0.389903000
1	1.697903000	2.137872000	-0.927489000
1	3.041779000	5.253365000	0.227229000
1	2.934171000	3.946168000	1.410304000
1	5.268681000	3.773304000	1.735068000
1	4.903468000	5.527165000	1.646469000
1	4.845230000	4.715310000	-4.626387000
1	4.206825000	4.217132000	-2.998028000
1	2.876471000	2.733702000	-4.111734000
1	3.548452000	2.883444000	-5.761841000
1	4.156277000	0.487475000	-5.812418000
1	2.427052000	0.714672000	-5.513324000
1	1.877988000	1.004620000	-3.130216000
1	1.653247000	-0.750199000	-3.345697000
1	3.266505000	-1.084458000	-1.347266000
1	1.705036000	-0.325737000	-0.970150000
1	8.996217000	-0.425977000	-4.460843000
1	10.739428000	-0.490171000	-4.006190000
1	9.378883000	1.405135000	0.559092000
1	5.942230000	3.005764000	-6.017285000
1	6.088833000	1.313699000	-5.390434000
1	5.381959000	-1.047005000	-5.812345000
1	5.484248000	-2.637526000	-5.071007000
1	6.145900000	-2.475116000	-2.387543000
1	2.421810000	1.915663000	0.692100000
1	10.254150000	2.816707000	1.264903000
1	6.313646000	-0.256422000	-3.539311000
1	7.681873000	-0.940863000	-1.473599000
1	7.801250000	2.218795000	1.847391000
1	4.387904000	3.047541000	-0.904278000
1	4.187634000	0.661089000	-0.335684000
1	8.721686000	2.981075000	-1.242204000
8	6.405816000	0.936532000	-1.057821000

[TREN₃CuᴵCuᴵCuᴵᴵ(μ_3-O)] – BP86/def2-SVP (C, H, O, N)/def2-TZVP (Cu)

2, 2

29	5.113601000	0.579796000	-2.423412000
7	3.416344000	0.075222000	-3.714160000
6	3.495152000	-1.378380000	-4.024000000
1	3.120133000	-1.935554000	-3.142043000
1	2.816326000	-1.641528000	-4.869412000
6	4.909727000	-1.851175000	-4.339291000
7	5.832736000	-1.508324000	-3.244264000
7	5.108129000	2.608988000	-4.112997000
6	6.257924000	2.349894000	-4.977066000
7	7.510572000	2.550797000	-4.246704000
29	8.041408000	0.982797000	-2.282325000
29	6.197588000	2.922971000	-0.652406000
7	7.960702000	3.116538000	0.816342000
6	9.332713000	3.219660000	0.287810000
7	9.685306000	2.091716000	-0.551806000
7	8.177109000	-1.228943000	-2.634919000
6	7.221777000	-1.808268000	-3.587275000
1	7.423134000	-1.369017000	-4.586354000
6	9.579668000	-1.467009000	-3.031345000
1	10.195712000	-1.518237000	-2.112721000
1	9.715593000	-2.445852000	-3.547367000
6	10.077503000	-0.346307000	-3.949980000
7	9.966616000	0.993277000	-3.312555000
7	3.247547000	0.661011000	-0.804892000
6	2.182785000	-0.053394000	-1.518208000
6	2.141107000	0.349639000	-2.998236000
6	3.499469000	0.867374000	-4.971369000
6	3.823667000	2.352022000	-4.775912000
6	5.167724000	3.974925000	-3.598192000
7	6.412325000	4.201743000	-2.857734000
7	5.837123000	4.983253000	0.037104000
6	7.049690000	5.410806000	0.783833000
6	7.613920000	4.280532000	1.651187000
1	6.869512000	3.961764000	2.407415000
1	8.488825000	4.668101000	2.224485000
1	7.816652000	5.722979000	0.048223000
1	6.836477000	6.307252000	1.411893000
6	5.589354000	5.854755000	-1.140211000
1	4.531337000	5.723427000	-1.444106000
1	5.690881000	6.931529000	-0.863213000
6	6.506316000	5.574413000	-2.334178000
6	7.564875000	3.914160000	-3.715853000
6	8.665976000	2.242506000	-5.101902000
6	9.981924000	2.069900000	-4.337590000
6	11.097106000	1.177532000	-2.358460000
1	12.049648000	1.348278000	-2.913336000
1	11.229850000	0.227371000	-1.802579000
6	10.893408000	2.303608000	-1.347499000
1	10.790457000	3.279942000	-1.869720000
1	11.827555000	2.388276000	-0.739229000
1	10.242536000	3.017880000	-3.827836000
1	10.795971000	1.894090000	-5.080196000
1	8.426684000	1.311063000	-5.657815000

1	8.829908000	3.025997000	-5.885052000
1	7.619776000	4.659223000	-4.567470000
1	8.482997000	4.032831000	-3.107042000
1	7.564608000	5.742334000	-2.042938000
1	6.285718000	6.337727000	-3.122611000
6	4.666726000	5.005429000	0.955084000
6	3.500727000	4.151708000	0.474930000
7	3.916938000	2.763691000	0.228313000
6	2.831496000	1.993803000	-0.382548000
1	2.504994000	2.554544000	-1.284050000
1	3.091050000	4.551674000	-0.476791000
1	2.671396000	4.237765000	1.217762000
1	4.999807000	4.627422000	1.941980000
1	4.319338000	6.050867000	1.126593000
1	5.073846000	4.727580000	-4.439807000
1	4.305885000	4.127217000	-2.918109000
1	3.034614000	2.828322000	-4.157974000
1	3.760639000	2.847610000	-5.777948000
1	4.270325000	0.401324000	-5.617324000
1	2.542922000	0.791906000	-5.541001000
1	1.932577000	1.435111000	-3.072406000
1	1.289200000	-0.164334000	-3.502281000
1	2.364921000	-1.142484000	-1.416782000
1	1.169362000	0.125532000	-1.082040000
1	9.470602000	-0.337442000	-4.876211000
1	11.126403000	-0.552993000	-4.266366000
1	10.057667000	3.375725000	1.134176000
1	6.221299000	3.014399000	-5.893976000
1	6.226661000	1.299093000	-5.327240000
1	5.287698000	-1.362486000	-5.261776000
1	4.878045000	-2.943684000	-4.561083000
1	7.385530000	-2.913843000	-3.686546000
1	1.933267000	1.948144000	0.295040000
1	9.392372000	4.135648000	-0.338268000
1	5.570300000	-2.048211000	-2.405646000
1	8.005272000	-1.619660000	-1.699077000
1	7.877202000	2.250259000	1.363614000
1	4.173965000	2.325360000	1.125457000
1	3.568837000	0.114865000	0.003371000
1	9.789111000	1.242538000	0.020631000
8	6.474696000	1.163979000	-1.251286000

[TREN₃CuᴵCuᴵᴵCuᴵᴵ(μ₃-O)] – BP86/def2-SVP (C, H, O, N)/def2-TZVP (Cu)

3, 3

29	5.013514000	0.642931000	-2.445526000
7	3.370342000	0.079773000	-3.764293000
6	3.501299000	-1.367388000	-4.095789000
1	3.095849000	-1.957383000	-3.249704000
1	2.879667000	-1.632801000	-4.981157000
6	4.947675000	-1.768680000	-4.339857000
7	5.804839000	-1.386192000	-3.189495000
7	5.091639000	2.552374000	-4.021035000
6	6.245253000	2.285569000	-4.893939000
7	7.515811000	2.492293000	-4.178846000
29	8.129092000	1.094591000	-2.239055000

29	6.158894000	2.985397000	-0.669338000
7	7.848373000	3.055874000	0.768780000
6	9.206555000	3.135575000	0.207034000
7	9.548084000	2.012951000	-0.674142000
7	8.163024000	-1.107790000	-2.530103000
6	7.210131000	-1.677776000	-3.496651000
1	7.431122000	-1.242985000	-4.492029000
6	9.559760000	-1.424091000	-2.932943000
1	10.184184000	-1.449687000	-2.018900000
1	9.641192000	-2.436850000	-3.387548000
6	10.080029000	-0.379666000	-3.922754000
7	10.003054000	0.991123000	-3.346917000
7	3.412823000	0.649856000	-0.913602000
6	2.279685000	-0.092213000	-1.531313000
6	2.114014000	0.311263000	-2.998331000
6	3.435506000	0.910444000	-4.998465000
6	3.804537000	2.370954000	-4.735709000
6	5.174391000	3.936186000	-3.527525000
7	6.427832000	4.168431000	-2.793195000
7	5.841734000	5.025905000	0.038130000
6	7.058573000	5.406559000	0.807650000
6	7.572982000	4.230229000	1.640124000
1	6.824026000	3.926360000	2.397048000
1	8.475426000	4.545806000	2.210111000
1	7.838222000	5.732491000	0.091252000
1	6.859899000	6.282835000	1.465305000
6	5.624528000	5.905070000	-1.142721000
1	4.561784000	5.813446000	-1.445503000
1	5.767582000	6.977212000	-0.872694000
6	6.534230000	5.573267000	-2.325734000
6	7.567537000	3.874199000	-3.679061000
6	8.642661000	2.200630000	-5.098749000
6	9.994158000	2.041859000	-4.401431000
6	11.131424000	1.203009000	-2.396269000
1	12.071965000	1.447057000	-2.939978000
1	11.323269000	0.248960000	-1.865269000
6	10.826726000	2.289992000	-1.376996000
1	10.728574000	3.278753000	-1.873365000
1	11.685202000	2.382415000	-0.673824000
1	10.291930000	2.999374000	-3.930569000
1	10.768294000	1.834094000	-5.175101000
1	8.386878000	1.267773000	-5.643960000
1	8.748180000	2.987625000	-5.885016000
1	7.581846000	4.597607000	-4.544747000
1	8.503235000	4.024259000	-3.105528000
1	7.595405000	5.743057000	-2.048142000
1	6.317330000	6.296997000	-3.148327000
6	4.652553000	5.043282000	0.936061000
6	3.532622000	4.151002000	0.424859000
7	4.025623000	2.772988000	0.175498000
6	2.958390000	1.961154000	-0.421814000
1	2.549764000	2.528165000	-1.282423000
1	3.124636000	4.537550000	-0.532027000
1	2.688102000	4.173858000	1.150617000
1	4.967881000	4.691614000	1.938149000

1	4.275369000	6.080751000	1.079045000
1	5.092128000	4.661534000	-4.387558000
1	4.314540000	4.120652000	-2.854685000
1	3.019451000	2.851748000	-4.115877000
1	3.795480000	2.915223000	-5.710641000
1	4.175108000	0.448996000	-5.683908000
1	2.464351000	0.882760000	-5.543858000
1	1.856954000	1.387002000	-3.064887000
1	1.259035000	-0.239822000	-3.451257000
1	2.486983000	-1.177104000	-1.439252000
1	1.323469000	0.082224000	-0.988341000
1	9.472386000	-0.401251000	-4.848106000
1	11.120682000	-0.628703000	-4.229877000
1	9.957506000	3.233142000	1.031664000
1	6.202706000	2.947919000	-5.806356000
1	6.208942000	1.236498000	-5.245530000
1	5.350376000	-1.256318000	-5.238473000
1	4.992159000	-2.859465000	-4.557940000
1	7.371091000	-2.781430000	-3.589660000
1	2.113625000	1.828312000	0.300599000
1	9.276376000	4.065018000	-0.393501000
1	5.527432000	-1.964747000	-2.380454000
1	7.979519000	-1.513775000	-1.601396000
1	7.770595000	2.195598000	1.329407000
1	4.272138000	2.355677000	1.087239000
1	3.777301000	0.104274000	-0.119625000
1	9.685699000	1.174129000	-0.088048000
8	6.452142000	1.246907000	-1.369009000

[TREN$_3$Cu^{II}Cu^{II}Cu^{II}(μ_3-O)] – BP86/def2-SVP (C, H, O, N)/def2-TZVP (Cu)

4, 4

29	4.991974000	0.732780000	-2.547108000
7	3.364416000	0.084940000	-3.778646000
6	3.494433000	-1.374536000	-4.087621000
1	3.085363000	-1.950454000	-3.234629000
1	2.869935000	-1.643707000	-4.968500000
6	4.939684000	-1.769071000	-4.323370000
7	5.790180000	-1.313320000	-3.185936000
7	5.093598000	2.496603000	-3.997332000
6	6.270367000	2.247922000	-4.858375000
7	7.541970000	2.472847000	-4.131124000
29	8.127298000	1.158401000	-2.355872000
29	6.168398000	3.068639000	-0.751028000
7	7.809573000	3.056339000	0.727388000
6	9.181456000	3.107412000	0.190815000
7	9.503235000	2.007546000	-0.730333000
7	8.158358000	-1.045940000	-2.527131000
6	7.193381000	-1.659967000	-3.457056000
1	7.436223000	-1.315951000	-4.481915000
6	9.552001000	-1.405002000	-2.937855000
1	10.182242000	-1.440966000	-2.028666000
1	9.599552000	-2.424449000	-3.378832000
6	10.076510000	-0.380949000	-3.940629000
7	10.009477000	0.995510000	-3.359258000
7	3.456886000	0.658138000	-0.959429000

6	2.294113000	-0.080299000	-1.546998000
6	2.106150000	0.327203000	-3.005934000
6	3.432161000	0.895147000	-5.031126000
6	3.812251000	2.347635000	-4.767722000
6	5.158135000	3.888854000	-3.494378000
7	6.406410000	4.147162000	-2.745325000
7	5.842040000	5.036448000	0.034923000
6	7.069103000	5.416226000	0.802160000
6	7.566075000	4.230080000	1.623558000
1	6.822838000	3.930018000	2.386920000
1	8.481690000	4.515101000	2.186201000
1	7.847884000	5.746420000	0.086556000
1	6.865153000	6.289859000	1.460130000
6	5.600324000	5.925512000	-1.139444000
1	4.532025000	5.839666000	-1.422757000
1	5.752081000	6.994164000	-0.863670000
6	6.495937000	5.587361000	-2.325577000
6	7.561578000	3.863118000	-3.629591000
6	8.671955000	2.227075000	-5.090859000
6	10.023304000	2.060775000	-4.404950000
6	11.135486000	1.187118000	-2.390486000
1	12.078290000	1.424421000	-2.931149000
1	11.315107000	0.226253000	-1.869107000
6	10.824376000	2.268200000	-1.372722000
1	10.777473000	3.269904000	-1.848200000
1	11.648455000	2.319192000	-0.626627000
1	10.337616000	3.009253000	-3.926520000
1	10.794590000	1.844729000	-5.178058000
1	8.414814000	1.310790000	-5.660913000
1	8.744287000	3.045514000	-5.843959000
1	7.552158000	4.577135000	-4.495465000
1	8.494454000	4.039840000	-3.061843000
1	7.558578000	5.782570000	-2.076057000
1	6.251243000	6.267679000	-3.173623000
6	4.656717000	5.040651000	0.950034000
6	3.546300000	4.147445000	0.432035000
7	4.077745000	2.785531000	0.136409000
6	2.999232000	1.946778000	-0.407843000
1	2.503092000	2.513329000	-1.221357000
1	3.108016000	4.549100000	-0.504640000
1	2.717611000	4.120496000	1.174515000
1	4.982692000	4.687040000	1.947242000
1	4.283502000	6.077770000	1.098287000
1	5.083376000	4.600381000	-4.358770000
1	4.287418000	4.069033000	-2.836476000
1	3.022627000	2.848546000	-4.171357000
1	3.858859000	2.895662000	-5.736520000
1	4.163500000	0.416862000	-5.713792000
1	2.457853000	0.867828000	-5.569238000
1	1.850174000	1.403217000	-3.076006000
1	1.253552000	-0.225191000	-3.459512000
1	2.489422000	-1.166851000	-1.452353000
1	1.357666000	0.106814000	-0.977096000
1	9.470191000	-0.400319000	-4.867268000
1	11.117317000	-0.628500000	-4.245072000

1	9.915816000	3.132291000	1.033007000
1	6.231795000	2.920808000	-5.755819000
1	6.250301000	1.204315000	-5.222756000
1	5.339786000	-1.305145000	-5.248854000
1	5.000579000	-2.869352000	-4.476467000
1	7.321063000	-2.769903000	-3.455305000
1	2.221383000	1.767054000	0.373925000
1	9.302692000	4.060302000	-0.362481000
1	5.494365000	-1.839555000	-2.346699000
1	7.986327000	-1.418029000	-1.580642000
1	7.706695000	2.193015000	1.281877000
1	4.373186000	2.368071000	1.034752000
1	3.850507000	0.092839000	-0.191869000
1	9.598273000	1.144987000	-0.168339000
8	6.450609000	1.284085000	-1.417582000

[**TREN**$_4$Cu^{I}Cu^{I}Cu^{II}(μ_3-OH)] – BP86/def2- TZVP (TD-DFT)

3, 2

29	9.863709000	-0.255723000	10.292554000
6	10.996198000	1.975354000	12.070077000
1	11.009247000	2.886877000	12.700143000
1	12.011053000	1.879665000	11.655274000
6	8.394522000	-1.357951000	12.903464000
1	7.912575000	-2.129739000	13.534778000
1	8.092595000	-0.389376000	13.329232000
7	7.892816000	-1.394897000	11.512450000
6	9.905498000	-1.535335000	13.002691000
1	10.196914000	-1.512594000	14.068425000
1	10.188046000	-2.529058000	12.628443000
7	10.678965000	-0.518770000	12.233431000
7	11.664062000	-1.539717000	9.645162000
7	12.065839000	-0.142993000	7.738207000
7	10.868347000	-2.238593000	7.454234000
6	10.681852000	0.782202000	12.966313000
1	11.415535000	0.755193000	13.792111000
1	9.700541000	0.909767000	13.440207000
6	11.427041000	-2.684149000	8.746803000
1	10.721391000	-3.370771000	9.232890000
1	12.383882000	-3.230268000	8.573150000
6	7.869488000	-2.766267000	10.993029000
1	7.216418000	-3.409952000	11.633127000
1	8.883266000	-3.188673000	11.014811000
6	12.082067000	-0.995383000	12.046313000
1	12.475399000	-1.422054000	12.986130000
1	12.708463000	-0.122883000	11.817099000
6	11.802554000	-1.255963000	6.841092000
1	11.341095000	-0.880102000	5.920946000
1	12.749456000	-1.783781000	6.563662000
6	12.638072000	-0.643691000	8.975244000
1	12.868770000	0.204208000	9.632619000
1	13.587265000	-1.211572000	8.803081000
6	12.363314000	1.645696000	5.957453000
1	12.087599000	0.954393000	5.150228000
1	13.178325000	2.273903000	5.537934000
6	12.204642000	-2.034433000	10.937301000

1	13.263140000	-2.338398000	10.844876000
1	11.645727000	-2.944036000	11.203832000
6	12.966250000	0.856304000	7.122064000
1	13.266756000	1.545121000	7.925146000
1	13.902905000	0.384603000	6.759948000
29	8.702366000	-1.652336000	7.771688000
6	10.739917000	-3.388253000	6.516339000
1	11.649199000	-4.017716000	6.522337000
1	10.668836000	-2.964932000	5.503717000
6	7.394857000	-4.168657000	9.101675000
1	6.604674000	-4.779748000	9.579532000
1	8.352281000	-4.618290000	9.405667000
7	7.388331000	-2.776360000	9.604639000
6	7.218453000	-4.253454000	7.590769000
1	7.220178000	-5.315876000	7.287668000
1	6.235404000	-3.853949000	7.310064000
7	8.252059000	-3.494233000	6.832302000
7	7.214861000	-0.850763000	5.830471000
7	8.609598000	1.040664000	5.406815000
7	6.541636000	1.340543000	6.642776000
6	9.529505000	-4.267559000	6.806790000
1	9.481000000	-5.071846000	6.050631000
1	9.646750000	-4.768952000	7.776325000
6	6.082530000	0.039031000	6.102565000
1	5.428087000	-0.446095000	6.840381000
1	5.487319000	0.217436000	5.173478000
6	6.024859000	-2.225177000	9.583361000
1	5.342101000	-2.879762000	10.181194000
1	5.651344000	-2.206024000	8.550520000
6	7.774170000	-3.256183000	5.436355000
1	7.355140000	-4.187551000	5.015129000
1	8.648212000	-3.005856000	4.820058000
6	7.504236000	1.941928000	5.681483000
1	7.888163000	2.869412000	6.122072000
1	6.956656000	2.207012000	4.741098000
6	8.089357000	-0.193984000	4.843498000
1	8.930023000	-0.856679000	4.598821000
1	7.514700000	-0.012626000	3.897536000
6	10.407617000	2.797693000	5.103654000
1	9.729009000	3.619106000	5.368236000
1	11.056322000	3.203153000	4.297868000
6	6.726711000	-2.150674000	5.329262000
1	6.395559000	-2.088928000	4.274503000
1	5.829874000	-2.419329000	5.908369000
6	9.601100000	1.648027000	4.497327000
1	10.276769000	0.838359000	4.183313000
1	9.126301000	2.022479000	3.566691000
29	7.158111000	1.128257000	8.846880000
8	8.851378000	0.136057000	8.622385000
6	5.387653000	2.271853000	6.762782000
1	4.771943000	2.267856000	5.843496000
1	5.801486000	3.287524000	6.849266000
6	4.613268000	-0.354338000	10.070969000
1	3.984521000	-0.847535000	10.838310000
1	4.188648000	-0.648092000	9.098945000

7	6.006374000	-0.852643000	10.104899000
6	4.505395000	1.153132000	10.265351000
1	3.437766000	1.437399000	10.267220000
1	4.899720000	1.428169000	11.252638000
7	5.248070000	1.941203000	9.241585000
7	7.869196000	2.897880000	10.228261000
7	9.777036000	3.353388000	8.859463000
7	10.074835000	2.120060000	10.919291000
6	4.490892000	1.963103000	7.955470000
1	3.675900000	2.707542000	7.998122000
1	4.005410000	0.987623000	7.826170000
6	8.767107000	2.621324000	11.368701000
1	8.286735000	1.864398000	12.004481000
1	8.899749000	3.552346000	11.972786000
6	6.524587000	-0.862005000	11.479286000
1	5.855095000	-1.468687000	12.139473000
1	6.541944000	0.163571000	11.872634000
7	11.178739000	2.441302000	6.302162000
6	5.459492000	3.336250000	9.732359000
1	4.530342000	3.733246000	10.178285000
1	5.682589000	3.969852000	8.863544000
6	10.672572000	3.089564000	9.975105000
1	11.608257000	2.660712000	9.597428000
1	10.924299000	4.037686000	10.517402000
6	8.535482000	3.903527000	9.367139000
1	7.879577000	4.155901000	8.523339000
1	8.698406000	4.837310000	9.964318000
6	11.542249000	3.638522000	7.071755000
1	12.354632000	3.369975000	7.759526000
1	11.960118000	4.438051000	6.423372000
6	6.586956000	3.429677000	10.753219000
1	6.688198000	4.480456000	11.081520000
1	6.330941000	2.853114000	11.655149000
6	10.388442000	4.256563000	7.865101000
1	9.584375000	4.565586000	7.180776000
1	10.761834000	5.189483000	8.335733000
1	9.434888000	0.686981000	8.049087000

[**TREN**$_4$Cu^{I}Cu^{II}Cu^{II}(μ_3-OH)] − BP86/def2- TZVP (TD-DFT)

4, 3

29	11.335532000	5.561258000	4.697933000
29	8.965119000	7.918370000	4.633196000
29	10.784921000	7.414099000	7.401208000
8	10.730231000	7.342440000	5.391752000
7	9.601658000	4.305787000	5.913186000
7	7.029813000	8.308150000	3.899175000
7	13.401160000	5.559503000	5.643785000
7	9.568134000	7.902492000	2.447341000
7	8.587901000	9.829380000	5.860954000
7	13.898996000	7.892185000	6.169954000
7	10.817242000	10.653486000	5.504129000
7	11.824082000	3.613733000	4.072882000
7	8.827917000	5.861894000	7.608814000
7	12.843888000	6.511488000	7.830235000
7	12.003851000	8.060406000	2.439214000

7	10.259138000	9.604626000	7.637565000
7	7.809035000	5.863488000	5.401357000
7	10.593006000	7.343613000	9.503238000
7	13.484446000	10.128058000	4.116902000
7	10.964562000	5.887885000	2.440322000
6	8.832687000	9.837002000	7.319098000
6	14.318335000	6.717565000	5.422672000
6	13.302045000	5.311117000	7.100235000
6	13.849898000	7.579865000	7.586690000
6	9.703921000	6.505471000	1.974771000
6	10.762776000	8.676379000	1.997320000
6	6.025334000	7.408828000	4.542013000
6	8.337969000	4.504391000	5.181463000
6	12.085941000	6.710405000	1.912499000
6	7.577771000	6.036620000	6.846988000
6	9.335141000	4.505255000	7.350433000
6	8.505515000	6.025135000	9.054182000
6	12.080056000	3.659203000	2.600672000
6	13.183638000	8.840751000	1.981640000
6	11.082829000	10.633492000	6.933827000
6	9.409891000	10.922269000	5.275417000
6	9.738224000	6.194726000	9.926836000
6	14.798067000	9.626855000	4.537536000
6	11.045542000	4.507373000	1.875074000
6	7.137558000	10.102151000	5.628197000
6	14.026838000	4.371006000	4.977902000
6	10.082301000	2.906945000	5.732732000
6	8.372672000	8.539775000	1.806574000
6	6.712916000	9.735270000	4.213219000
6	10.708835000	2.665513000	4.368416000
6	13.058429000	3.210634000	4.812072000
6	14.821937000	9.034936000	5.946933000
6	9.985465000	8.636213000	9.944026000
6	13.356230000	10.198859000	2.657310000
6	10.481005000	9.803457000	9.106326000
6	12.792143000	6.181799000	9.287073000
6	11.635329000	11.684212000	4.816715000
6	11.969865000	7.196163000	10.067759000
6	6.517466000	5.974820000	4.664162000
6	13.136111000	11.396799000	4.766973000
6	7.058219000	8.087045000	2.421944000
1	8.514891000	10.817908000	7.739130000
1	8.220684000	9.053524000	7.785759000
1	15.351169000	6.402646000	5.708833000
1	14.315674000	6.947249000	4.350434000
1	12.596182000	4.490998000	7.285384000
1	14.297583000	5.003360000	7.490710000
1	14.835861000	7.234382000	7.982888000
1	13.569739000	8.484940000	8.142602000
1	8.860627000	5.910864000	2.350337000
1	9.673569000	6.485746000	0.861765000
1	10.727366000	8.757807000	0.883665000
1	10.685612000	9.688059000	2.412661000
1	5.787257000	7.817501000	5.531771000
1	5.082215000	7.418837000	3.968611000

1	8.511656000	4.363880000	4.107223000
1	7.588524000	3.745599000	5.508546000
1	12.043824000	6.687767000	0.796576000
1	13.041290000	6.265379000	2.220610000
1	6.809579000	5.306759000	7.197120000
1	7.193915000	7.047363000	7.038135000
1	8.597280000	3.748676000	7.708946000
1	10.271630000	4.350479000	7.900881000
1	7.850100000	6.903510000	9.140753000
1	7.918495000	5.168319000	9.435427000
1	13.086689000	4.066012000	2.438914000
1	12.084114000	2.640194000	2.176174000
1	14.067532000	8.212812000	2.168207000
1	13.153162000	9.004748000	0.886060000
1	12.138306000	10.390408000	7.106983000
1	10.872417000	11.626756000	7.399653000
1	9.228673000	10.980199000	4.194583000
1	9.081751000	11.890768000	5.726309000
1	10.352229000	5.285700000	9.904579000
1	9.419195000	6.323458000	10.976024000
1	15.135178000	8.874194000	3.811287000
1	15.573156000	10.420366000	4.509497000
1	10.046680000	4.052990000	1.951180000
1	11.288508000	4.532363000	0.798059000
1	6.568520000	9.518445000	6.366143000
1	6.894262000	11.162363000	5.817872000
1	14.396504000	4.709210000	3.999400000
1	14.913033000	4.026151000	5.539297000
1	10.813615000	2.711052000	6.530863000
1	9.264050000	2.178391000	5.881825000
1	8.495408000	9.627179000	1.917568000
1	8.353116000	8.339270000	0.720454000
1	7.225948000	10.369979000	3.479735000
1	5.633189000	9.927657000	4.091020000
1	9.953885000	2.764657000	3.577114000
1	11.069051000	1.623228000	4.316679000
1	12.757884000	2.818857000	5.792964000
1	13.568807000	2.381607000	4.292760000
1	14.546663000	9.805766000	6.682281000
1	15.868821000	8.753437000	6.179382000
1	8.893964000	8.546432000	9.875441000
1	10.212295000	8.826539000	11.006903000
1	12.502164000	10.845663000	2.412754000
1	14.233613000	10.689342000	2.186552000
1	11.561902000	9.946232000	9.247141000
1	9.997378000	10.732914000	9.455837000
1	12.361262000	5.175022000	9.385649000
1	13.806751000	6.125678000	9.719026000
1	11.234816000	11.770676000	3.795318000
1	11.496337000	12.681731000	5.279522000
1	12.453938000	8.181040000	10.047821000
1	11.921870000	6.893481000	11.127633000
1	6.670163000	5.536826000	3.666579000
1	5.726963000	5.368833000	5.144445000
1	13.550766000	11.393785000	5.784266000

1	13.612618000	12.264046000	4.265301000
1	6.893461000	7.018939000	2.230208000
1	6.223248000	8.618437000	1.933931000
1	11.389742000	8.002306000	5.060312000

8. Reference

(1) Yakelis, N. A.; Bergman, R. G. Safe Preparation and Purification of Sodium Tetrakis[(3,5-Trifluoromethyl) Phenyl]Borate (NaBArF$_{24}$): Reliable and Sensitive Analysis of Water in Solutions of Fluorinated Tetraarylborates. *Organometallics* **2005**, *24*, 3579.

(2) Stoll, S.; Schweiger, A. EasySpin, a Comprehensive Software Package for Spectral Simulation and Analysis in EPR. *J. Magn. Reson.* **2006**, *178*, 42.

(3) Sequoia, E.; Laboratoire, O. N.; Organique, P.; Gabriel, S. General Expression of the linear Potential Sweep voltammogram in the Case of diffusionless Electrochemical Systems. **1979**, *101*, 19.

(4) Sivasankaran, U.; Vikraman, A. E.; Thomas, D. Nanomolar Level Determination of Octyl Gallate in Fats and Oils. *Food Anal. Methods* **2016**, 2115.

(5) Nicholson, R. S. Theory and Application of Cyclic Voltammetry for Measurement of Electrode Reaction Kinetics. *Anal. Chem.* **1965**, *37*, 1351.

(6) Lavagnini, I.; Antiochia, R.; Magno, F. An Extended Method for the Practical Evaluation of the Standard Rate Constant from Cyclic Voltammetric Data. *Electroanalysis* **2004**, *16*, 505.

(7) Gennari, M.; Pøcaut, J.; Debeer, S.; Neese, F.; Collomb, M.; Duboc, C. A Fully Delocalized Mixed-Valence Bis-µ-(Thiolato) Dicopper. *Angew. Chem. Int. Ed.* **2011**, *50*, 5662.

(8) Weaver, M. J. An Alternative Approach to the Intercomparison of Electron-Transfer Reactivities at Metal Surfaces and in Homogeneous Solution1. *J. Phys. Chem.* **1990**, *94*, 8608.

(9) Neese, F. Software Update : The ORCA Program System, Version 4.0. *Wiley Interdiscip. Rev. Comput. Mol. Sci.* **2018**, *8*, 4.

(10) Viktor N. Staroverov and Gustavo E. Scuseria. Comparative Assessment of a New Nonempirical Density Functional : Molecules and Hydrogen-Bonded Complexes. *J. Chem. Phys.* **2004**, *119*, 12129.

(11) Marenich, A. V; Cramer, C. J.; Truhlar, D. G. Universal Solvation Model Based on Solute Electron Density and on a Continuum Model of the Solvent Defined by the Bulk Dielectric Constant and Atomic Surface Tensions. *J. Phys. Chem. B* **2009**, *113*, 6378.

(12) Johnson, E. R.; Becke, A. D. A Post-Hartree-Fock Model of Intermolecular Interactions: Inclusion of Higher-Order Corrections. *J. Chem. Phys.* **2006**, *124*, 174104.

(13) Grimme, S.; Ehrlich, S.; Goerigk, L. Effect of the Damping Function in Dispersion Corrected Density Functional Theory. *J. Comput. Chem.* **2011**, *32*, 1456.

(14) Koepke, S. J.; Light, K. M.; Vannatta, P. E.; Wiley, K. M.; Kieber-Emmons, M. T. Electrocatalytic Water Oxidation by a Homogeneous Copper Catalyst Disfavors Single-Site Mechanisms. *J. Am. Chem. Soc.* **2017**, *139*, 8586.